Synthetic and computational efforts toward the understanding and development of novobiocin-derived inhibitors of Hsp90

By

Donna J. Lubbers

B.S., Saint Mary's College, Notre Dame, 2005

Submitted to the Department of Medicinal Chemistry and the Faculty of the Graduate School of The University of Kansas in partial fulfillment of the requirements for the degree of Masters of Science.

Thesis Committee:

_____
(Chairperson)

_____

_____

Date defended: _____

The Thesis Committee for Donna J. Lubbers certifies that this is the approved version of the following thesis:

Synthetic and computational efforts toward the understanding and development of novobiocin-derived inhibitors of Hsp90

Thesis Committee:

_____
(Chairperson)

_____

_____

Date approved: _____

Abstract

As *C*-terminal inhibitors of a 90-kDa heat shock protein (Hsp90), novobiocin and its derivatives are a significant part of an emerging class of cancer chemotherapeutic agents. Previous studies have shown that analogues of the coumarin and benzamide moieties of novobiocin exhibit more than a 1000-fold improvement in activity over the parent compound. This thesis describes synthetic efforts toward the completion of noviose mimics to determine moieties that are critical for binding or can be altered for improved activity. Additionally, in the absence of a co-crystal structure for the Hsp90 *C*-terminus, there is a need to develop an accurate model to assist in efficient drug design. This work describes the use of molecular modeling and docking software to design new, potentially useful models of *C*-terminal interactions.

Acknowledgments

I would be remiss if I did not, first and foremost, thank my advisor, Professor Brian Blagg, whose research goals originally brought me to this university. Many faculty and staff members shaped my graduate school experience at KU, and I especially thank Professors Barbara Timmermann and Paul Hanson for their additional participation and support as members of my thesis committee.

My greatest mentors in the laboratory setting have been Joseph Burlison and Gang Shen, two of the most skilled synthetic chemists I have ever had the honor of meeting. I will be eternally grateful to them for their patience and guidance, as well as the encouragement, friendship, and memories that I will always hold dear. I have had the privilege of working with many brilliant minds and kind hearts, and give sincere thanks to Natalia Ortuzar, Geraldine Calvet, and the other Blagg Lab members.

My parents have given me unconditional love and support for all of my decisions and have encouraged me to do not only that at which I am best, but that about which I am most passionate. They will always be the two greatest role models in my life. My brothers, grandparents, and other family members and friends have been a solid support network as well, and their thoughts and prayers have given me comfort throughout. Love to Thomas Alan, who continues to help me remember what is most important, and never stops believing that I can achieve absolutely anything.

Finally, I dedicate this thesis to my Aunt Paula- the amazing woman who has always shared my love of the sciences and of life in general, and who constantly inspires me to see the best in every situation. Love and thanks to you all.

Table of Contents

List of Figures

List of Schemes

List of Tables

Introduction and Background

Heat shock proteins are molecular chaperones that are upregulated in response to stressful cellular conditions, such as exposure to toxins, hypoxia, or elevated temperatures caused by inflammation or other means. Of these, the 90-kDa heat shock protein, Hsp90, is an emerging target for the treatment of diseases due to its ability to refold denatured proteins or to fold nascent polypeptides, as well as its role in solubilizing protein aggregates that are often associated with neurodegenerative diseases. Of particular note is the fact that Hsp90 client proteins are intertwined with all of the six hallmarks of cancer, as defined by Hanahan and Weinberg,[1] leading to the hypothesis that inhibition of Hsp90 could simultaneously disrupt multiple pathways associated with malignancy, producing very potent and selective cancer chemotherapeutics. Natural product discoveries and associated synthetic and biological efforts have paved the way for the significant progress that has been made within the past decade in this area of research, and continue to shape our understanding of Hsp90 and its implications as a therapeutic target.

Geldanamycin and Derivatives. Originally discovered as an antimicrobial compound in 1970, geldanamycin (GDM, Fig. **1**) is a member of the ansamycin family of antibiotics and has been shown to exhibit activity against the growth and development of protozoa. The initial isolate was extracted from an actinomycete soil sample from Kalamazoo, Michigan. GDM was screened against a number of protozoae both *in vitro* and *in vivo*, and demonstrated antimicrobial activity against *Alternizaria, Pythium, Botrytis* and *Penicillium.* The minimal inhibitory

concentration (MIC) of GDM was most notable for *Tetrahymena pyriformis* at 2 mg/mL and *Crithidia fasciculata* at 4 mg/mL.[2]

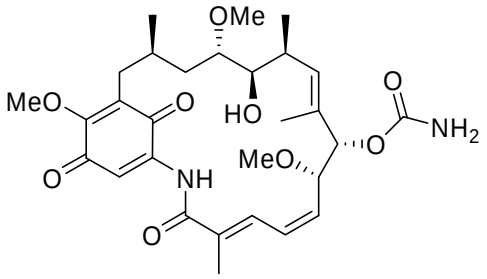

Figure 1. Structure of geldanamycin (GDM).

Upon further testing, GDM was found to possess antiproliferative activity against a wide range of tumor cell lines, which was believed to result from direct inhibition of v-Src, a tyrosine specific kinase that is involved in several signal transduction pathways and regulates the growth and proliferation of transformed cells.[3] Although GDM did significantly diminish v-Src kinase activity in cells,[4] it was inactive against the purified protein, suggesting that GDM was indirectly inhibiting v-Src kinase activity via an alternative mechanism.[5] Through affinity purification, Whitesell and Neckers determined that GDM was reversibly binding a protein, Hsp90.[6] It was proposed that the Hsp90 molecular chaperone was responsible for the conformational maturation of v-Src and, therefore, the activity was dependent upon Hsp90. These researchers demonstrated that upon administration of GDM, v-Src and other Hsp90-dependent protein substrates were degraded in cell lysates, thereby linking client protein degradation to Hsp90 inhibition. Subsequent studies have

shown that upon Hsp90 inhibition, Hsp90-dependent client proteins become substrates for the ubiquitin-proteasome pathway.[7]

In 1997, Stebbins and coworkers reported the first co-crystal structure of GDM bound to Hsp90 (Fig. **2**).[8] At the time, GDM was believed to bind to the client protein binding site. However, studies revealed that GDM bound to the *N*-terminal ATP-binding site of Hsp90, and that in the presence of GDM, the inherent ATPase activity of Hsp90 was diminished.[9] The co-crystal structure also revealed two key features of GDM when bound to Hsp90. First, GDM binds Hsp90 in a bent conformation and contains a *cis*-amide bond,[8] distinctive from the native crystal structure in which it adopts a relatively flat conformation with a *trans*-amide bond.[10,11] Additionally, the quinone ring binds Hsp90 towards the surface of the protein, suggesting that modifications at the 17-position should not affect inhibitory activity.[12]

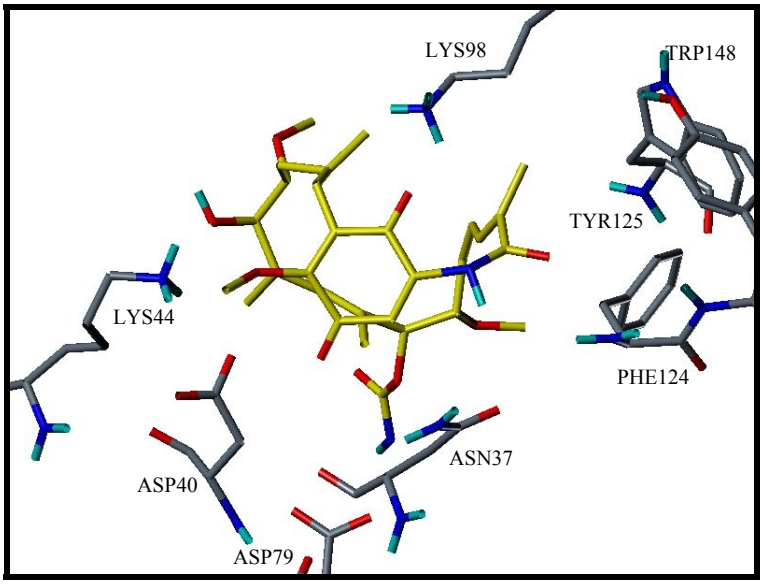

Figure 2. Co-crystal structure of GDM bound to yeast Hsp90.[12]

In vivo studies with GDM proved to be problematic as the redox-active quinone and the labile nature of the 17-methoxy substituent led to hepatotoxicity.[13,14] In an effort to decrease the electron-deficient nature of the quinone ring and to remove the labile 17-methoxy group, researchers prepared numerous GDM analogues. The most potent of these was 17-(allylamino)-17-demethoxygeldanamycin (17-AAG, Scheme 1).[15] 17-AAG has demonstrated improved inhibitory activity and decreased hepatotoxicty compared to GDM.[15,16] Consequently, 17-AAG entered clinical trials as the first Hsp90 inhibitor for the treatment of cancer and more recently advanced to Phase II trials.[17,18]

Despite improvements over GDM, 17-AAG still exhibits poor solubility in animal studies, suggesting that further modifications are needed to alleviate these undesired properties. In 2004, researchers at Kosan Biosciences reported the synthesis and evaluation of 17-DMAG, which exhibits significantly greater aqueous solubility than 17-AAG and may have potential use as an orally administered drug (Scheme 1).[19,20] In contrast to 17-AAG, 17-DMAG contains a tertiary ammonium group that is ionized at physiological pH. Consequently, 17-DMAG has also entered clinical trials and is expected to complement 17-AAG.

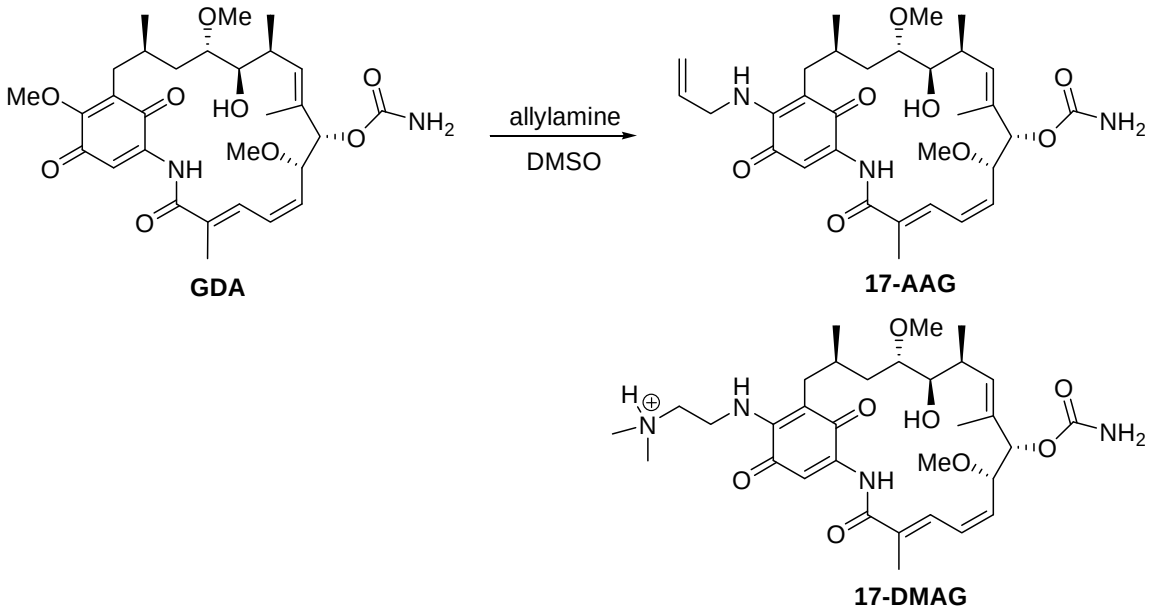

Scheme 1. Synthesis of 17-AAG and the structure of 17-DMAG.

To improve selectivity of 17-AAG and to occupy both *N*-terminal ATP-binding sites of the homodimeric protein, researchers prepared GDM dimers.[21] The four-carbon tether (Fig. **3**) produced by Rosen and coworkers exhibited the greatest inhibitory activity for this series of compounds and demonstrated high selectivity toward the Her2 family of receptors. Subsequently, Kuduk and coworkers attempted to prepare compounds for selective inhibition of Hsp90-dependent client proteins such as the estrogen receptor (ER).[22] After identification of the optimal tether for linking GDM with estradiol, these hybrids were prepared and evaluated against the MCF-7 human breast cancer cell line. Compared to 17-AAG, these compounds exhibited enhanced selectivity towards the ER and Her2, but exhibited reduced activity against Raf-1. Shortly thereafter, these researchers developed a GDM-

testosterone hybrid to target the androgen receptor for potential use in prostate cancer.[23] Results obtained from these studies suggested that these molecules may have therapeutic applications for advanced breast and prostate cancers, respectively.

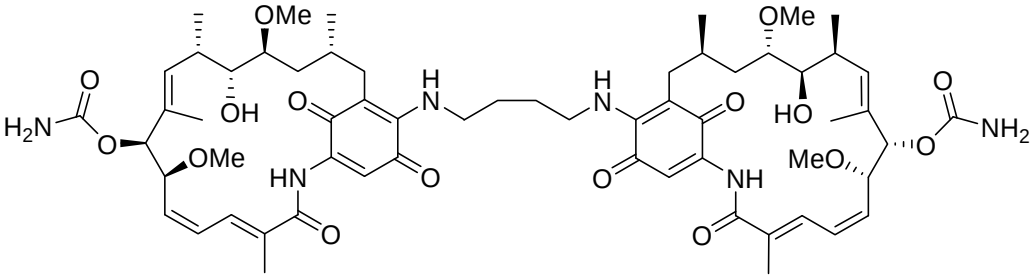

GDM dimer

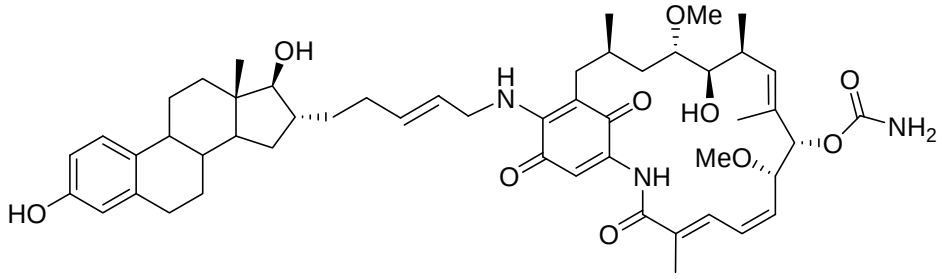

Estradiol-geldanamycin hybrid

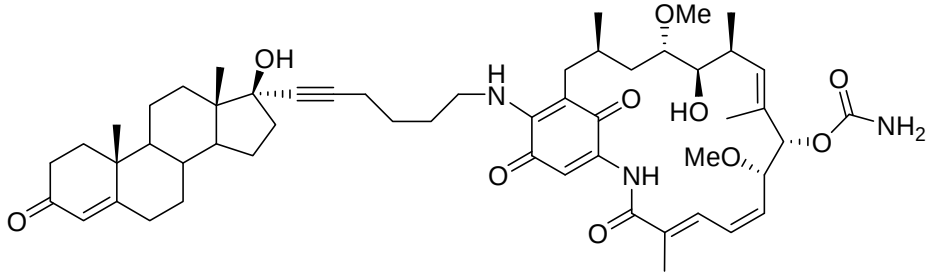

Testosterone-geldanamycin hybrid

Figure 3. Structures of a GDM dimer, estradiol-GDM, and testosterone-GDM.

The ability of GDM to modulate Hsp90 function makes it an ideal ligand for the exploitation of low affinity ligands for other therapeutic targets. For example,

Chiosis and colleagues prepared heterodimers of GDM and LY294002, a small-molecule inhibitor of phosphoinositol-3 kinase (PI3K), in hopes that the bifunctional ligand could regulate PI3 kinase activity. These heterodimers, with linkers varying in composition, length, and site of attachment showed improved efficacy and specificity toward the inhibition of PI3K and PI3K-related proteins. One of the identified derivatives, LY6-GM (Fig. **4**), exhibited a two-fold increase in selectivity for DNA-dependent protein kinase (DNA-PK) versus PI3K.[24]

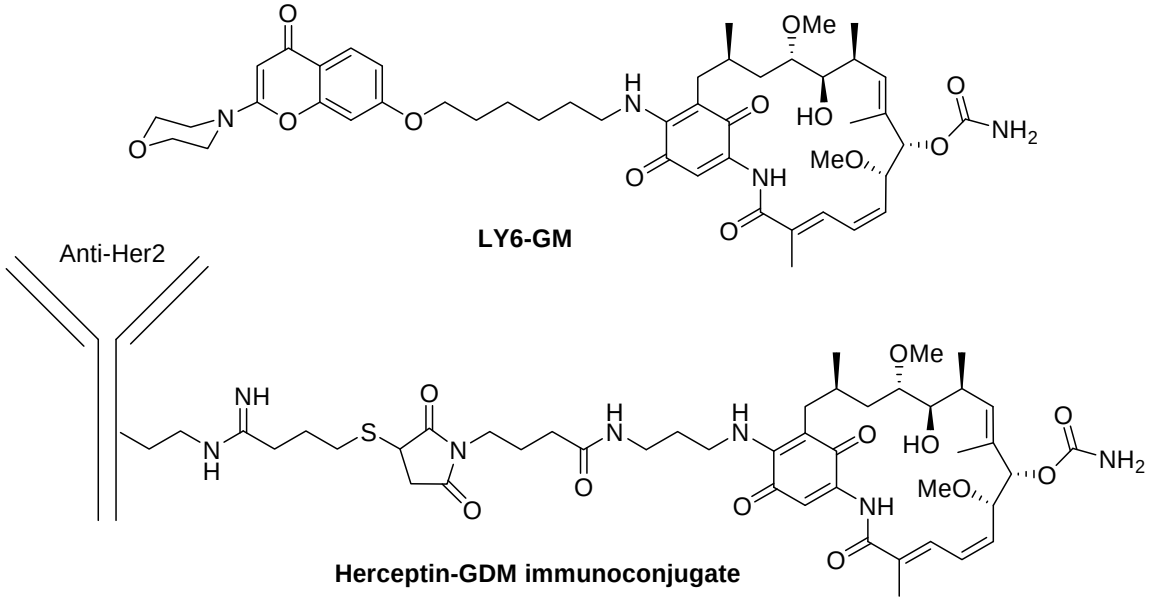

Figure 4. Structures of LY6-GM and H-GDM.

The anti-Her2 monoclonal antibody (mAb) Herceptin has shown clinical efficacy for carcinomas that overexpress Her2, an Hsp90 client protein.[25] In an attempt to improve the anticancer activity of Herceptin and other anti-Her2 mAbs, the GDM derivative 17-aminopropylamino-geldanamycin (17-APA-GA) was attached to lysine residues on the mAbs through a stable linker.[26,27] The Herceptin-GDM

immunoconjugate (H-GDM, Fig. **4**) exhibited 10–200 fold increased antiproliferative activity against various cancer cell lines. In addition, H-GDM treatment prolonged survival of xenograft-bearing mice compared to Herceptin treatment alone through decreased tumor growth and induced tumor regression. These results suggest that immunoconjugates of this type can provide a complementary approach to treat certain types of cancer.

Attempts to identify structure–activity relationships for GDM have proven difficult. To date, few total syntheses of GDM have been reported, requiring from 20 to more than 40 linear steps to complete.[28] Researchers at Kosan Biosciences have taken a complementary approach toward the preparation of GDM analogues through modification of the GDM biosynthetic pathway to produce novel bioengineered geldanamycin analogues (Fig. **5**).[29] The most important finding from their studies was that KOSN1559 exhibited higher affinity for Hsp90 compared to GDM. This is especially significant because the phenol is not redox-active and is likely to augment the liability associated with the quinone compounds that are currently in clinical trials.

Compound	IC_{50} SkBr3 (nM)	K_d (nM)
GDM	41	670
17-AAG	33	1300
KOSN1558	>5000	1000
KOSN1559	860	160
KOSN1630	4900	3000
KOSN1631	3200	5000
KOSN1859	480	5200
KOSN1877	470	660

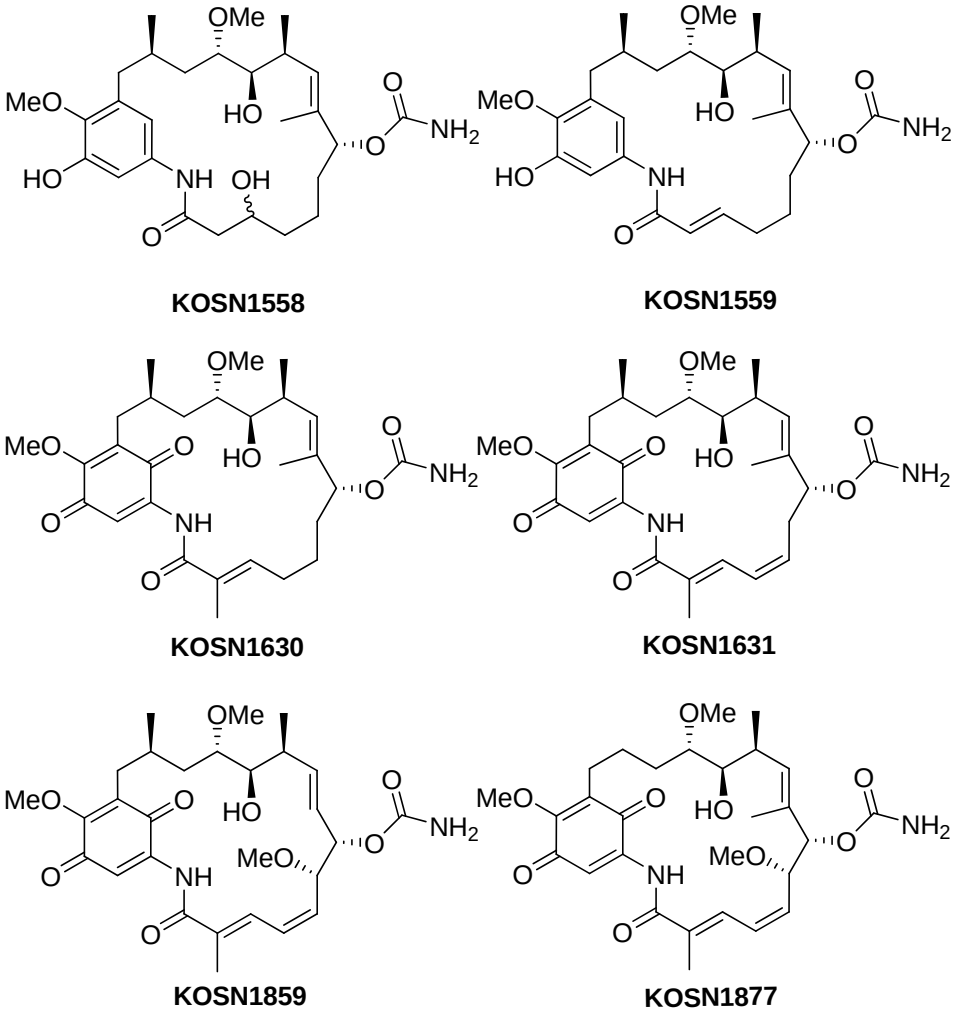

Figure 5. Bioengineered GDM analogues.

In addition to their uses as anti-cancer agents, GDM and its derivatives have been utilized to probe the mechanism by which Hsp90 inhibition regulates tumor cell

growth. 17-AAG has shown differential selectivity towards cancer cells and studies have revealed that it accumulates in malignant cells at higher concentrations than the surrounding media.[30] However, this could not be directly correlated to Hsp90 inhibition because 17-AAG inhibits purified Hsp90 at low micromolar concentrations, but manifests low nanomolar activity in tumor cell proliferation studies.[16] Consequently, studies were needed to identify the mechanism by which 17-AAG exhibits enhanced inhibitory activity in cells.

In 2003, Kamal and coworkers reported that 17-AAG exhibits higher affinity for the Hsp90 heteroprotein complex found in transformed cells.[31] Using immunoprecipitation techniques, Hsp90 was isolated from several tumor cell lines and was shown to exist as a heteroprotein complex composed of client proteins, co-chaperones, and partner proteins; whereas Hsp90 isolated from normal cells was found to reside as a homodimeric protein, uncomplexed to other proteins. The ATPase activities of homodimeric Hsp90 and the Hsp90 multiprotein complex were measured. Tumorigenic Hsp90 heteroprotein complexes were shown to have a higher ATPase activity than the homodimeric protein, and this increased activity correlated directly with its increased affinity for 17-AAG. Thus, tumor-derived Hsp90 has a higher affinity for *N*-terminal ligands than the homodimeric protein used in general ATPase assays.

GDM has also been used as a molecular probe in fluorescence polarization (FP) assays by the incorporation of fluorescent dyes onto the 17-position of the quinone ring.[32] These relatively small molecules tumble more slowly when bound to

Hsp90 than when floating freely in solution and can therefore be used to identify competitive inhibitors of the Hsp90 *N*-terminal ATP-binding site. These FP assays are more useful than other methods such as isothermal calorimetry, circular dichroism, or even filter binding assays that use [^{3}H]17-AAG because they do not require large quantities of protein or radioactive materials.[33] Two novel geldanamycin-derived fluorescent probes were reported by Chiosis and coworkers, GM-FITC and GM-BODIPY, Fig. (**6**).[32]

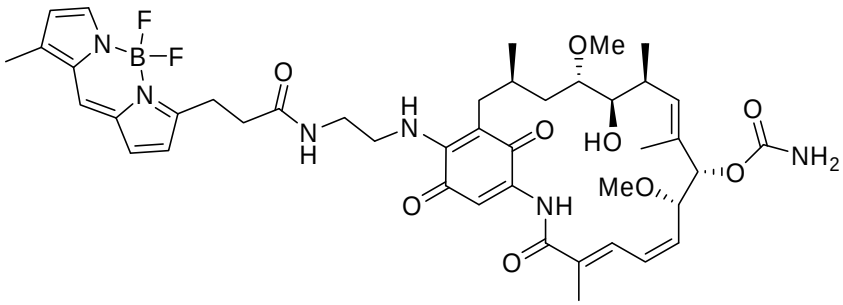

Figure 6. Structure of GM-BODIPY.

Biotinylated GDM (bGDM, Fig. **7**) has also been prepared and used for affinity purification and assay development. Introduction of a diamino group at the 17-position of the quinone ring allowed subsequent coupling of the primary amine with biotin. These compounds were used to identify other proteins that bound bGDM.[34] In addition, bGDM was used by Kamal and coworkers in competitive binding assays to measure binding affinities of 17-AAG for immunoprecipitated Hsp90 heteroprotein complexes.[32] This bGDM has also been used in fluorescence studies by researchers at the Genomics Institute of the Novartis Research Foundation,

where a time-resolved fluorescence resonance energy transfer (FRET)-based high-throughput screening assay was developed to screen a library of ~100,000 compounds.[34] Using this technique, the researchers identified several small molecules that exhibit binding affinities for Hsp90 in the high nanomolar range.

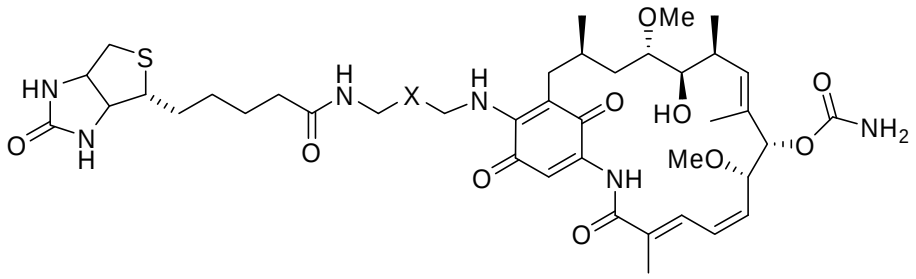

Figure 7. Structure of biotinylated GDM.

Although GDM and its derivatives have shown initial promise as cancer chemotherapeutics, an efficient synthetic procedure has not been developed that can be used to identify structure–activity relationships or improved analogues. In addition, the hepatotoxicity and redox-active nature of GDM derivatives represent major obstacles for increasing the activity for this family of compounds. Consequently, there remains a tremendous need to develop more efficacious compounds that lack these negative properties.

Radicicol and related compounds. Like GDM, radicicol (RDC, Fig. **8**) was also believed to be a specific v-Src kinase inhibitor prior to elucidation of Hsp90 as its biological target.[36] The 14-membered macrolide was isolated from the culture broth of *Monosporium bonorden* in 1953 as an antifungal antibiotic.[37] Subsequent

studies confirmed that RDC possessed the ability to suppress the transformation of Ras, Src and Mos oncogenes, which led to the development of RDC as an anticancer agent. Later studies demonstrated that this antitumor activity was based on its ability to bind and inhibit Hsp90 ATPase activity, which in cells resulted in the degradation of signaling proteins that served as nodes in oncogenic pathways.[36,38] RDC was shown to compete with GDM for binding to the *N*-terminus of purified human Hsp90 and to alter the cellular level of Hsp90-dependent client proteins in human breast cancer cell lines.[36] These experiments confirmed that like geldanamycin, RDC exerts its anticancer activity through inhibition of the Hsp90 protein folding machinery.

RDC exhibits a higher affinity for full-length homodimeric Hsp90 than GDM (K_d = 19 nM and 1.2 μM, respectively) and is significantly more potent against the purified recombinant Hsp90 ATPase assay.[12] Of note, the different K_d values obtained for GDM are a result of the different assays used to measure its ability to bind Hsp90. RDC is not redox active and does not exhibit hepatotoxicity like GDM and its derivatives.[39] In addition, RDC has demonstrated potent cytotoxicity against retinoblastoma-negative cells known to be resistant to 17-AAG.[40] However, RDC has not been shown to possess differential selectivity towards tumorigenic Hsp90 multiprotein complexes in the same manner as GDM derivatives. The native crystal structure of RDC and its bound conformation are identical, suggesting that the relatively inflexible ring system is likely to bind both the activated and unactivated forms of Hsp90 with equal affinity and thus prohibit differential inhibition of the tumorgenic heteroprotein complex.[12,41] In contrast to GDM, which exhibits an

entropic penalty upon Hsp90 binding due to conformational reorganization and isomerization of the amide bond, RDC binds Hsp90 with a favorable entropic binding energy resulting from the displacement of water from the ATP binding site.[12]

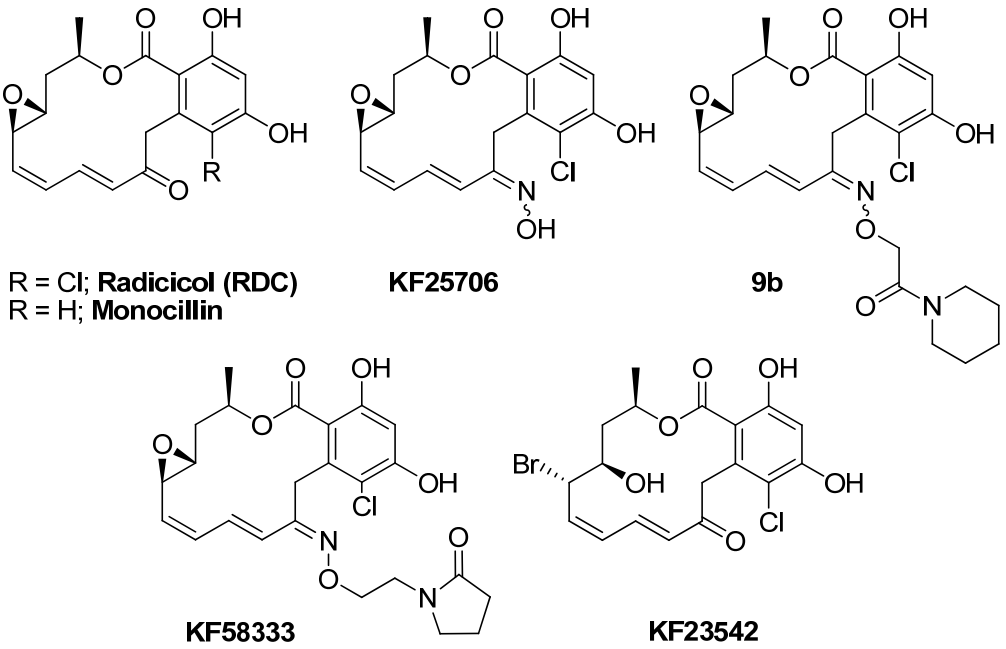

Figure 8. Radicicol and various analogues.

The crystal structure of RDC bound to yeast Hsp90 shows that the resorcinol ring provides key binding interactions with the protein, which appear essential for its high affinity (Fig. **9**).[12] The 3-hydroxyl forms a hydrogen bond with Asp79 and a conserved water molecule, mimicking key interactions of the natural adenine base. The 5-hydroxyl forms a hydrogen bond with Leu34. The chloro substituent partially fills a hydrophobic cavity that is important for biological activity. In fact, monocillin, which lacks the chlorine atom, manifests substantially lower affinity for Hsp90 than RDC.

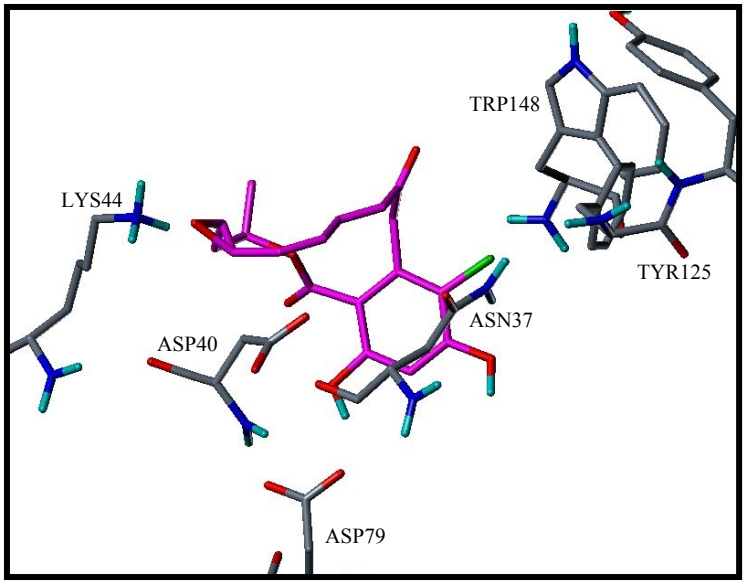

Figure 9. Co-crystal structure of RDC bound to yeast Hsp90.[12]

In contrast to GDM, RDC lacks antitumor activity *in vivo*.[42] It is thought that the allylic epoxide and the α,β,γ,δ-unsaturated ketone undergo nucleophilic addition that results in biologically inactive metabolites. It has been shown that thiol-derived nucleophiles inactivate RDC, presumably through this process.[43] In an attempt to decrease the electrophilic nature of these functionalities, 6-oxime and halohydrin derivatives of RDC were prepared and evaluated for anticancer potential (Fig. **8)**.[44,45]

Both KF25706[44] and 9b[45] were synthesized and evaluated as a mixture of both the *E*- and *Z*-isomers. These compounds manifested potent antiproliferative activity and induced the degradation of Hsp90-dependent client proteins *in vitro*. In addition, they exhibited significant activity *in vivo* against human tumor xenograft models. The most potent of these derivatives to date, 9b, demonstrated a 3–12 fold increase in

antiproliferative activity in various cancer cell lines and showed enhanced inhibition of v-Src activity compared to RDC (IC_{50} = 25 nM and 180 nM, respectively).[45] Purification of the *E*-oxime from the mixture of isomers led to identification of KF58333 as the biologically active inhibitor.[46] In fact, KF58333 maintained potent inhibition of tumor growth in xenograft models, while the Z-isomer was inactive. This data suggests the configuration at the 6-position is important for *in vivo* activity of oxime derivatives. The bromohydrin KF23542 displayed inhibitory activity comparable to RDC *in vitro*, however, its inactivity *in vivo* appears to result from its rapid conversion to the epoxide (RDC) and subsequent metabolic inactivation.[47]

Although RDC has been previously synthesized,[48] recent work by Danishefsky and coworkers has led to a succinct synthesis of this natural product and identification of the first structure–activity relationships for RDC and Hsp90.[40,49] Evaluation of the inhibitory activity of RDC analogues with varying stereochemistry demonstrated the importance of the natural configuration for inhibitory activity. In order to replace the problematic allylic epoxide with a more stable isostere, a cyclopropyl analogue of RDC was prepared (cycloproparadicicol, c-RDC, Fig **10**). The antiproliferative activity of c-RDC was comparable to RDC (IC_{50} = 43 and 23 nM, respectively) against MCF-7 cells.[40] In addition, only c-RDC with the same configuration as RDC demonstrated inhibitory activity.

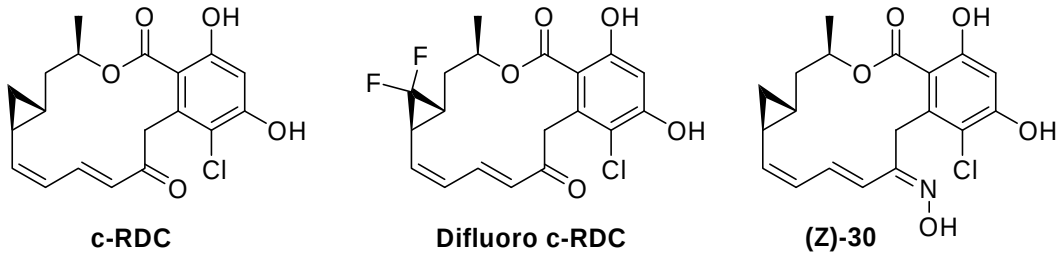

Figure 10. Cycloproparadicicol and various analogues.

Recent improvements toward the synthesis of RDC through use of the 'ynolide method' provided several new c-RDC analogues for elucidation of structure–activity relationships.[50] The co-crystal structure of RDC bound to Hsp90 suggests that the epoxide oxygen of RDC forms a hydrogen bond with Lys58. However, replacement of this moiety with a methylene group (c-RDC) resulted in only a two-fold decrease in inhibitory activity, suggesting that the conformation exerted on the macrocycle by the three-membered ring is more important than the hydrogen bonding interaction. This is further supported by the difluoro c-RDC derivative, which should provide complementary interactions with Lys58, however, this compound exhibited significantly lower activity (GI_{50} = 3 μM).[50] In contrast to the results described above for the 6-oxime derivatives of RDC, the *Z*-oxime of c-RDC[36] was 3-fold more active than the corresponding *E*-isomer.[50] Conformational analysis of RDC and its analogues suggest that the *Z*-isomer is predisposed to a bioactive conformation.[51] The *in vivo* inhibitory activity of these compounds has not yet been reported.

Other compounds in the 14-membered resorcinolic macrolide class have been prepared and evaluated for inhibitory activity (Fig. **11**). Both Aigialomycin D[50] and des-chloro Pochonin D[51] exhibit significantly decreased inhibitory activity compared

to RDC. Combined with the low activity demonstrated for monocillin, these data underline the importance of the chlorine atom for optimal inhibitory activity. Both Pochonin D[51] and A[50] are high affinity binders of Hsp90 (IC_{50} = 80 and 90 nM, respectively); however, *in vitro* activities for these compounds reside in the low micromolar range.

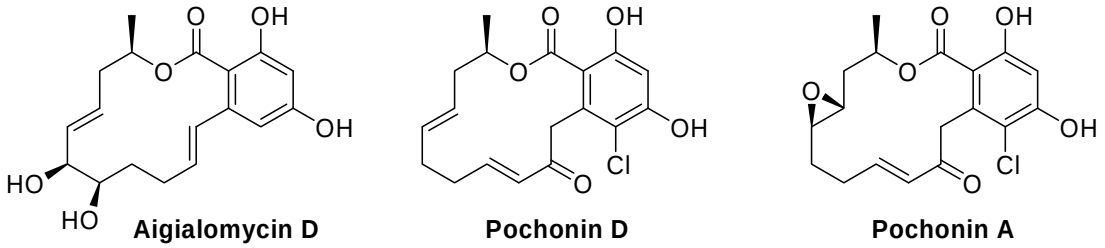

Figure 11. RDC-related macrolide Hsp90 inhibitors.

Both the ynolide approach by Danishefsky and coworkers to prepare RDC analogues and the polymer-assisted method used by Winssinger and colleagues to prepare Pochonin D and related derivatives have provided a platform upon which future analogues can be prepared and more efficacious compounds identified. Results from such studies may lead to useful alternatives to the redox-active geldanamycin derivatives that are currently in clinical trials.

Radicicol and geldanamycin chimeras. As stated previously, RDC and GDM are the most potent natural product *N*-terminal inhibitors of Hsp90 identified thus far. However, both molecules exhibit potential liabilities as a result of their electrophilic properties and/or redox-active behavior. In contrast to RDC, GDM derivatives have been shown to possess differential selectivity that appears directly

related to the bent conformation of GDM bound to Hsp90, which contains an isomerized *trans* to *cis* amide bond.[53,54] On the other hand, RDC retains the same conformation bound and unbound to Hsp90 and inhibits the Hsp90 homodimer ATPase activity at low nanomolar concentrations as compared to the low micromolar inhibitory activity of GDM.

Figure **12** shows the superimposed co-crystal structures of RDC and GDM bound to the *N*-terminus of yeast Hsp90.[12] The resorcinol ring of RDC occupies the same region as the carbamate of geldanamycin and the purine ring of ATP. However, the quinone rests at the protein–solution interface, in the same region as the catalytic residues required for ATP hydrolysis.[54] It has been proposed that these amino acids are involved in isomerization of the geldanamycin amide and, therefore, play a key role in the differential selectivity observed for this molecule. Unfortunately, only lengthy total syntheses of geldanamycin have been reported to date and improved analogues have not been published.[28] Therefore, it was proposed that one could use the high-affinity resorcinol ring as a surrogate for the GDM carbamate to create molecules that contain a macrocyclic ring system that incorporated the quinone and amide functionalities of GDM. Radanamycin, a chimera of radicicol and geldanamycin, was designed *in silico* to determine whether this hybrid could complement the binding interactions of each natural product. Radamide and radester were prepared and evaluated as *seco*-agents in an effort to determine the optimal tethers to connect the quinone and resorcinol moieties.

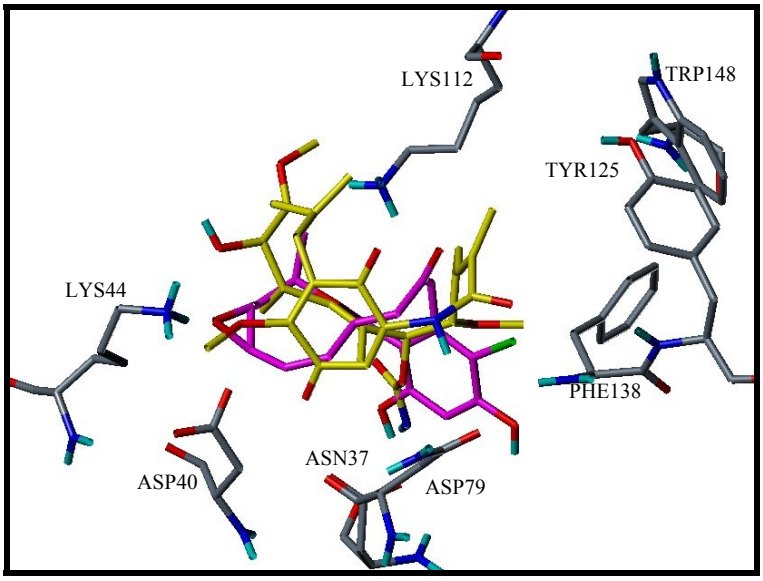

Figure 12. Superimposed co-crystal structures of radicicol (magenta) and geldanamcyin (yellow) bound to Hsp90.[12]

The first chimeric compound prepared, radamide, provided an efficient synthetic method through which numerous analogues could be prepared (Fig. **13**).[53] Upon evaluation of radamide in the Hsp90 ATPase assay, it was found that the quinone-containing compound exhibited an IC_{50} value of 5.9 μM, which compared well to that of geldanamycin (2.5 μM).[54] However, the quinone was not the most active compound. Instead, it was the hydroquinone that exhibited an IC_{50} value of 1.9 μM. An analogue that contained a trimethoxy substituted ring in lieu of the quinone resulted in an IC_{50} value greater than 50 μM, suggesting that detrimental interactions occur in the binding pocket despite its close proximity to the aqueous solution. The GI_{50} of these molecules in MCF-7 breast cancer cells was 23μM, 42 μM and 85 μM, for the hydroquinone, quinone and trimethoxy variants, respectively, suggesting that

the flexible linker connecting the resorcinol and quinone rings may lower the effectiveness of these compounds in cells.

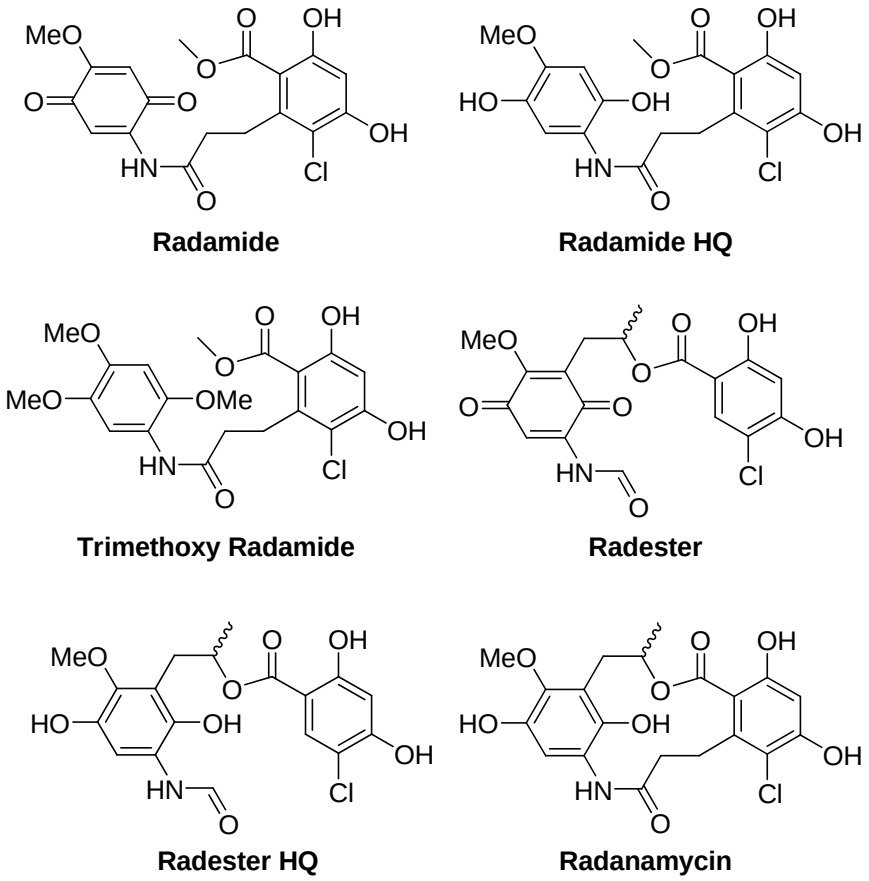

Figure 13. Chimeras of radicicol and geldanamycin.

Following the preparation of radamide, radester was synthesized to identify the optimal tether to connect the resorcinolic ester with the quinone.[57] A seven-step synthesis afforded the quinone, and the antiproliferative activity of both the hydroquinone and quinone was evaluated against MCF-7 cells. Once again, the hydroquinone was more active than the quinone (GI_{50} = 7 and 14 μM, respectively)

and these activities correlated directly to the degradation of Hsp90-dependent client proteins Her2 and Raf-1.

With an optimized ester and amide chain length identified, the macrocyclic radanamycin chimera was prepared and evaluated in MCF-7 breast cancer cells. This compound exhibited a GI_{50} value of 1.2 μM, which correlated directly with the degradation of Hsp90 clients Her2 and Akt.[58]

The ability to simultaneously elucidate structure–activity relationships for both GDM and RDC with these chimeric inhibitors proved useful for the preparation of improved analogues of the corresponding natural products. Recently, researchers at Infinity Pharmaceuticals determined that the hydroquinone of 17-AAG is the active species in cancer cells and that this compound maintains higher affinity for Hsp90 than the corresponding quinone. Consequently, the hydroquinone of 17-AAG became the first natural product-based Hsp90 inhibitor to enter Phase I clinical studies for the treatment of cancer.

***C*-terminal inhibitors.** In 2000, Neckers and coworkers made another significant contribution to the Hsp90 field of research. It had been previously noted that geldanamycin adopted a cup-shaped conformation when bound to the Hsp90 *N*-terminal ATP-binding pocket. Neckers and colleagues realized that novobiocin, a natural product used clinically in Europe as an antibiotic, exhibited a similar cup shape when bound to its cognate protein, DNA gyrase (Fig. **14**).

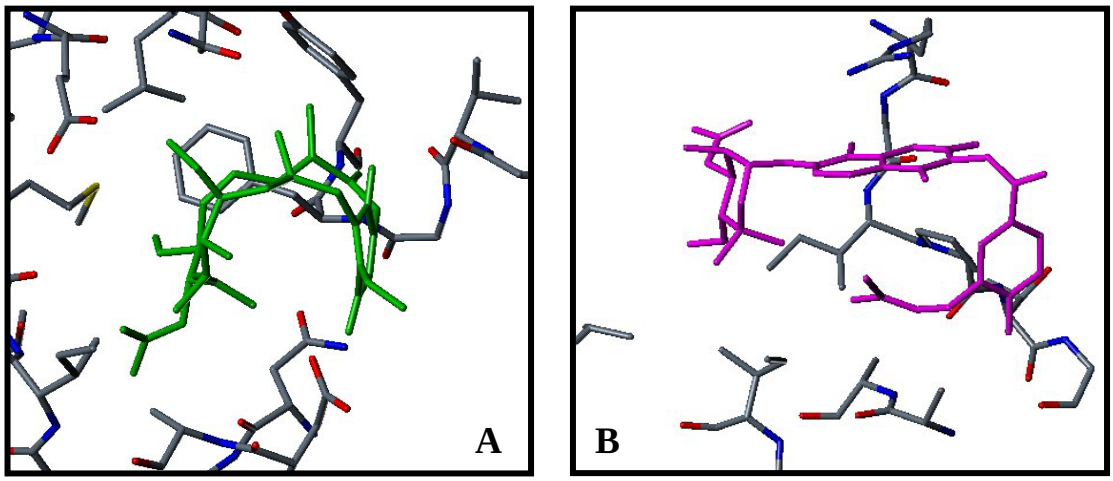

Figure 14. A) Geldanamycin (green) bound to Hsp90 and B) novobiocin (magenta) bound to DNA gyrase.

As members of the GHKL superfamily, which is composed of the proteins Gyrase, Hsp90, histidine Kinase, and MutL, these proteins share many common attributes with regard to the structure of their ATP-binding domains. It was hypothesized that novobiocin might, therefore, act as an Hsp90 inhibitor, which was subsequently proven via assays in which novobiocin was shown to bind both purified Hsp90 and Hsp90 from cell lysates. Furthermore, novobiocin was able to deplete Hsp90 client proteins $p185^{erbB2}$ and Raf-1 in a concentration-dependent manner.[59]

However, in subsequent studies with geldanamycin and radicicol, it appeared as though novobiocin did not compete with these inhibitors at the *N*-terminal ATP-binding site.[59] Following deletion/mutation analyses by Marcu *et. al*. using truncated fragments of Hsp90, it was concluded that novobiocin bound to a previously unrecognized binding site located within the *C*-terminal domain.[60] Thus began studies of a new class of small molecule inhibitors of the Hsp90 *C*-terminus.

In addition to novobiocin, which was the first identified inhibitor of the Hsp90 *C*-terminus, other aminocoumarin antibiotics such as clorobiocin and the dimeric compound, coumermycin A1, have also been shown to exhibit *C*-terminal inhibitory activity, demonstrating IC_{50} values of 350 μM and 70 μM, respectively, against MCF cells. Additionally, derrubone, a flavonoid natural product that was recently discovered to inhibit Hsp90 (IC_{50} value 14μM), is believed to bind the *C*-terminus.[61]

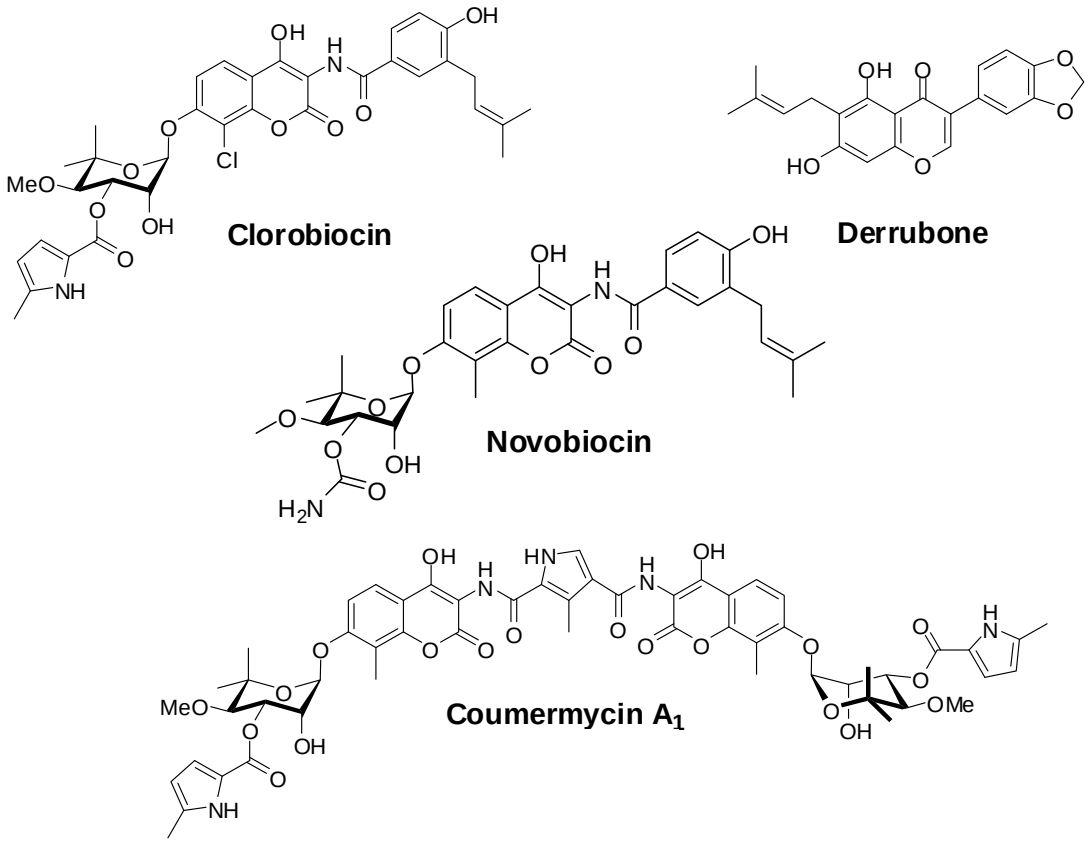

Figure 15. Natural product *C*-terminal Hsp90 inhibitors.

Novobiocin analogues have become promising lead compounds for a number of efforts toward the synthesis and development of highly potent and selective Hsp90

inhibitors. Further studies aimed toward the understanding of how these compounds interact with the *C*-terminus may provide clinically useful compounds that can be used as alternatives to Hsp90 *N*-terminal inhibitors.

Results and Discussion

Synthetic efforts toward new analogues of novobiocin. Since the identification of novobiocin as a *C*-terminal Hsp90 inhibitor in 2000, studies have been underway in the Blagg Laboratory to produce more efficacious and selective analogues of this natural product. The structure of this molecule can be considered as three separate moieties: the benzamide side chain, the central coumarin core, and the noviose sugar (Fig. **16**).

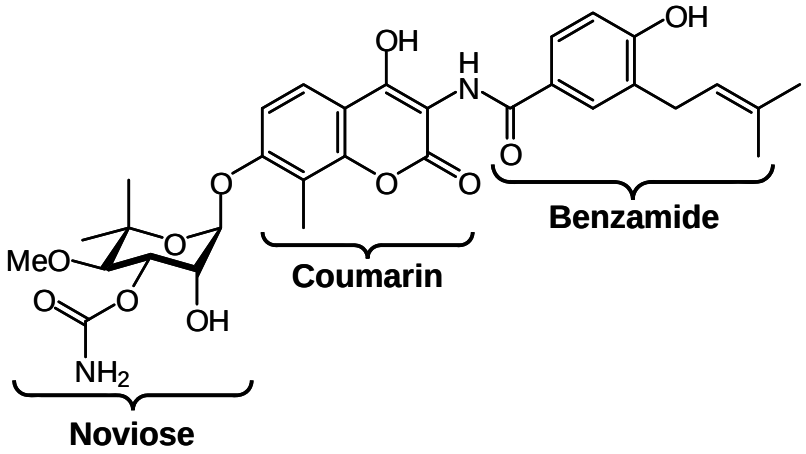

Figure 16. Novobiocin, a *C*-terminal Hsp90 inhibitor.

Early synthetic efforts by the Blagg laboratory indicated that the benzamide side chain was critical to growth inhibitory activity; derivatives lacking this functionality were shown to manifest neuroprotective activity. It was hypothesized that the mode of action was consistent with Hsp90 modulatory effects.[62] Later, derivitization of the benzamide side chain led to improved analogues exhibiting as

much as a 1000-fold increase in activity over the parent compound, novobiocin, against a range of cancer cell lines.[63]

Derivatives of the coumarin core were also designed in an attempt to create more potent inhibitors. It was determined in early studies that the hydroxyl group at the 4-position of the coumarin was detrimental to Hsp90 activity, and actually allowed for selectivity against DNA gyrase instead.[64] Upon analysis of initial SAR, it was also noted that a methyl group in the 8-position gave nearly a ten-fold improvement over the parent compound, which contains a hydrogen at the 8-position. Additionally, the natural product clorobiocin contains an 8-chlorocoumarin moiety which was twice as active as novobiocin against SKBr3 cells.

Further derivatives of the 8-position were therefore synthesized to determine the depth and characteristics of the binding pocket into which this moiety projects, including various 8-alkyl, -aryl, and –halide groups. Benzoyl protection of the glycine amine was followed by esterification using thionyl chloride and methanol. Upon treatment of the methyl ester with diformamide dimethyl acetal, it was possible to access the vinylogous carbamate, which was a common intermediate for the synthesis of the 8-R position coumarins via the corresponding 2-R position resorcinols (Scheme. **2**).

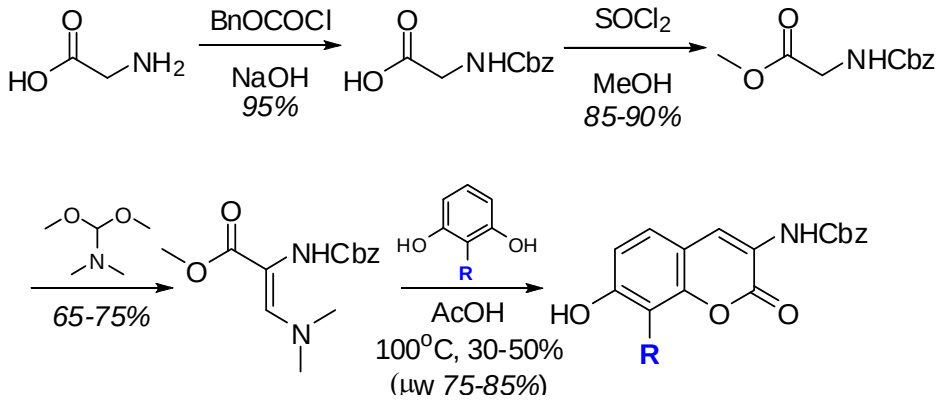

Scheme 2. General synthesis of 8-position coumarin derivatives.

With synthetic efforts and further evaluation underway to pursue more effective coumarin analogues, the final focus to complete preliminary SAR studies of novobiocin was to pursue the noviose appendage. Preliminary work reported by the Blagg Laboratory in 2005 showed that modifications to the 3'-carbame moiety of the sugar affected Hsp90 inhibitory activity, and it was hypothesized that further SAR would lead to significant improvements in efficacy.[62] Previously accessed by our laboratory for the construction of other analogues, noviose can be isolated after 11 steps in an overall yield of 8%.[65] The synthesis, as shown in Scheme **3**, involves harsh conditions, expensive reagents, and multiple purifications, effectively hindering synthetic progress. Therefore, the design and synthesis of simple sugar mimics was proposed to yield novel novobiocin derivatives exhibiting improved potency, selectivity, and ease of accessibility over those containing the noviose sugar.

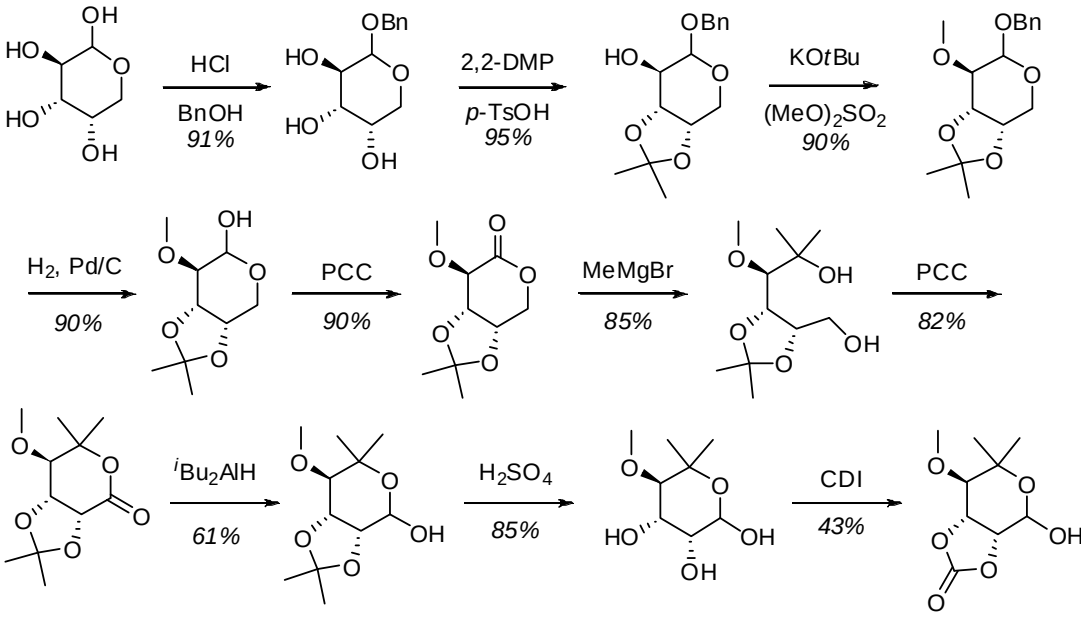

Scheme 3. Synthesis of noviose.

In order to determine accurate structure–activity relationships for sugar mimics, it was necessary to couple them to a common scaffold. We therefore chose the 8-methyl coumarin core, coupled to the biaryl acid that had produced consistent and potent inhibitory activity against several cancer cell lines. The synthesis of this scaffold (Scheme **4)**, involved acetate protection of the 7-position phenol of the coumarin moiety, followed by removal of the Cbz protecting group using standard hydrogenolysis conditions to afford free amine **3**. Simultaneously, Suzuki conditions were employed utilizing methyl 3-iodo-4-methoxybenzoate and 3-methoxyphenyl-boronic acid to yield the biaryl methyl ester shown. Hydrolysis of the ester occurred in near-quantitative yield using lithium hydroxide in a mixture of tetrahydrofuran,

water, and methanol, providing carboxylic acid **5,** for subsequent coupling to the previously described amine, which was carried out under standard peptide coupling conditions enlisting EDCI. The entire scaffold was then subjected to lithium hydroxide or triethylamine in order to solvolyze the cyclic carbonate and afford phenol **6** for coupling to sugar mimics.

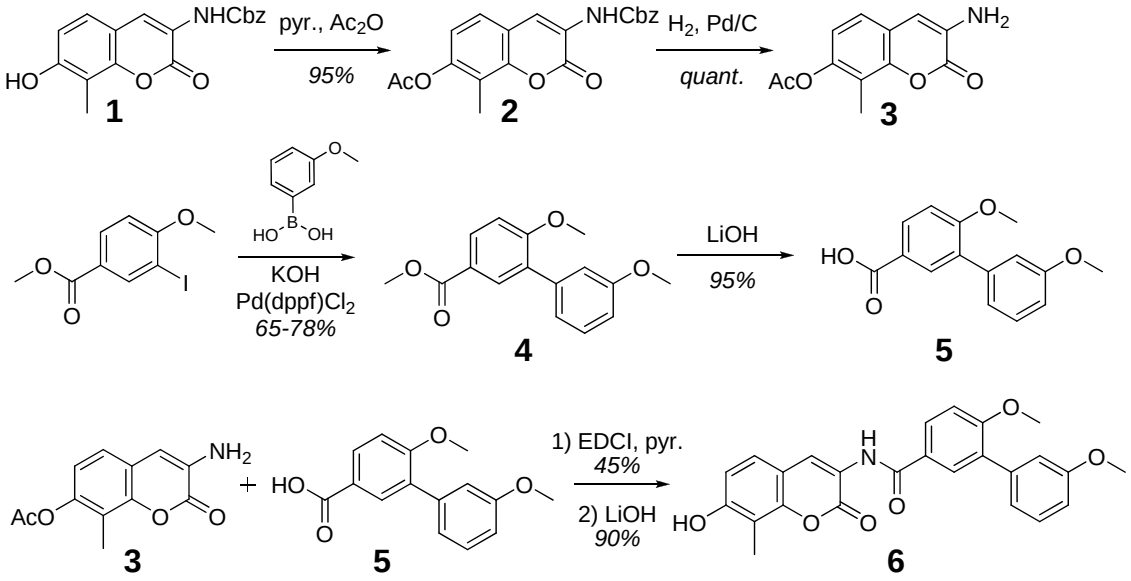

Scheme 4. Synthesis of scaffold.

Initial sugar analogues, completed by the O'Doherty laboratory at West Virginia University, were evaluated for anti-proliferative activity, with all three derivatives exhibiting increased potency over parent compound KU-111 (Fig. **17**). The data from these KU-111 derivatives indicated that the sugar moiety did, in fact, play a critical role in the binding interactions of novobiocin to Hsp90. Therefore, in

an effort to further elucidate structure-activity relationships, to streamline the overall syntheses of the novobiocin family *C*-terminal inhibitors, and to produce more efficacious small molecules, we set out to pursue a library of noviose mimics.

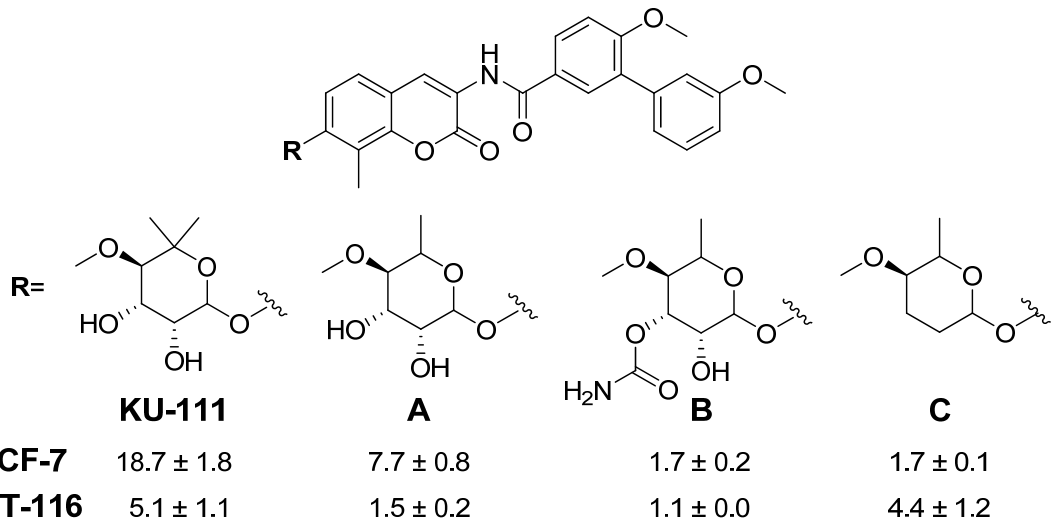

Figure 17. Anti-proliferative activity (in μM) of analogues with KU-111 scaffold.

We designed a library of racemic cyclohexanol derivatives, to be accessed via procedures between one and six steps in length, a significant improvement over the synthesis of noviose. The specific binding interactions of the parent compound are unknown, since a co-crystal structure has yet to be determined for any *C*-terminal inhibitors. These mimics, therefore, were designed with either nitrogen or oxygen heteroatoms at various positions within the ring structure to probe the hydrogen-bonding interactions with the binding pocket and to provide derivatives that exhibit improved solubility. Additionally, since all three derivatives from the original series

(Fig. **17**) exhibited increased inhibitory effects over KU-111 and contained a single methyl group instead of the gem-dimethyl moiety present on the parent compound, derivatives with both these variations, as well as a di-desmethyl derivative were designed. Finally, the initial series aimed to determine whether the diol was a necessary component for Hsp90 inhibition, therefore, derivatives with and without this functionality were proposed as well (Fig. **18**).

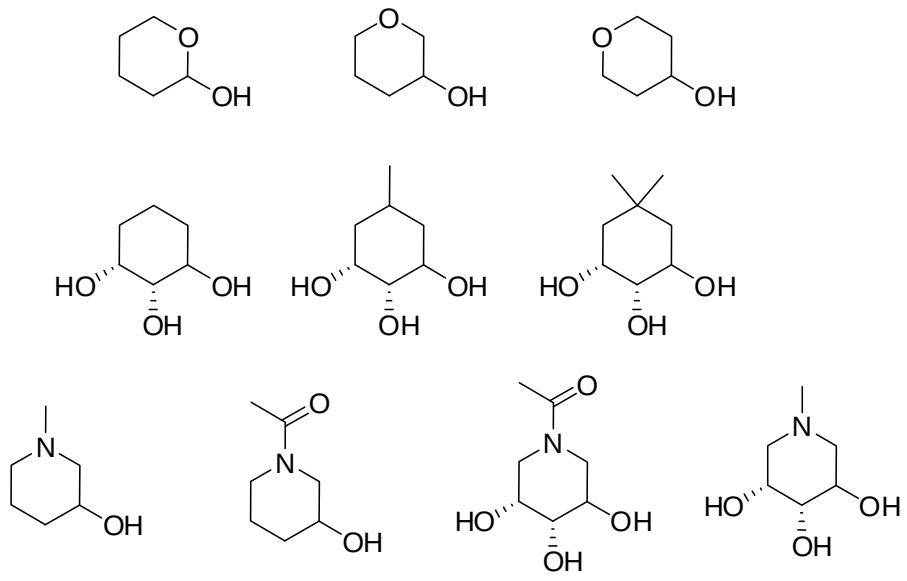

Figure 18. Library of sugar mimics.

Many of these simplified versions of the sugar moiety were accessible using common procedures (Scheme **5**), such as one-pot reductions with lithium aluminum hydride to produce compounds **7** and **8**, or via Luche conditions to yield **9**. An oxidation procedure afforded alcohol **10** from dihydropyran, and compounds **11** and **12** were purchased commercially. Compounds containing a double bond were

designed to be coupled to the scaffold and subsequently dihydroxylated to give the corresponding diols for comparison. The procedures utilized gave moderate to excellent yields, and all were significantly more succinct than the synthetic route to noviose.

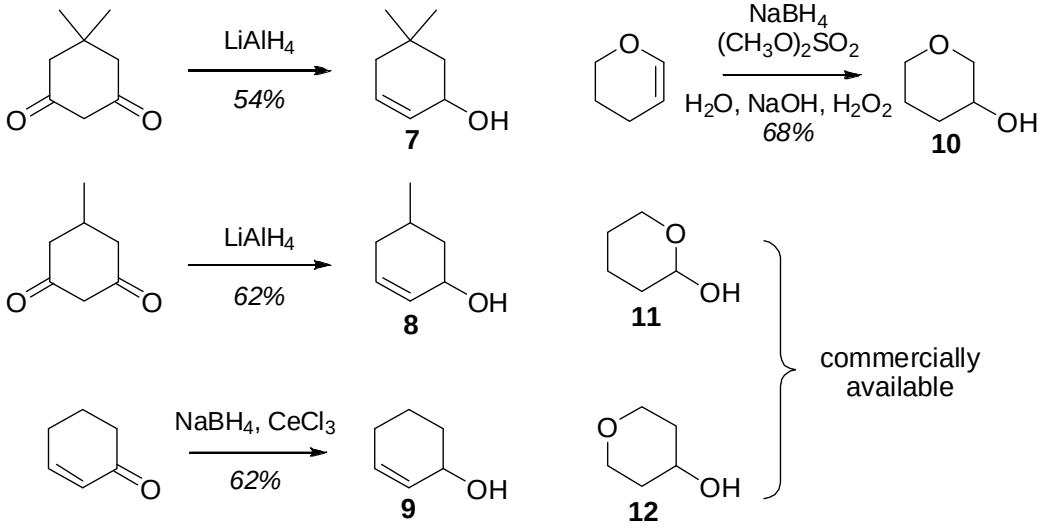

Scheme 5. Synthesis of sugar mimics.

While formylation and acetylation of nitrogen-containing derivatives **13** and **14** proceeded with great chemoselectivity in one step without the need for protection or deprotection (Scheme **6**), the two compounds that contained a double bond presented a greater synthetic challenge. Butadiene monoxide and allylamine were coupled using a catalytic amount of water to afford bis-alkene intermediate **15**. The route bifurcated at this point, and we used similar conditions as before to protect the secondary amine as either the N-methyl or N-acetyl moiety to make respective derivatives **16** and **17**. The alcohols were initially protected using *tert*-butyl dimethyl

silyl groups prior to ring-closing metathesis (RCM), but this was later found unnecessary, since RCM can occur readily in the present of an allylated alcohol, resulting in improved yields and fewer steps to achieve **18** and **19**.[66] RCM was also successful in much higher yields using Grubbs' second generation catalyst than with the first generation variant, which we hypothesized was the result of greater functional group tolerance. Additionally, only destabilized dichloromethane provided the solubility and the inert environment for these RCM reactions to occur.

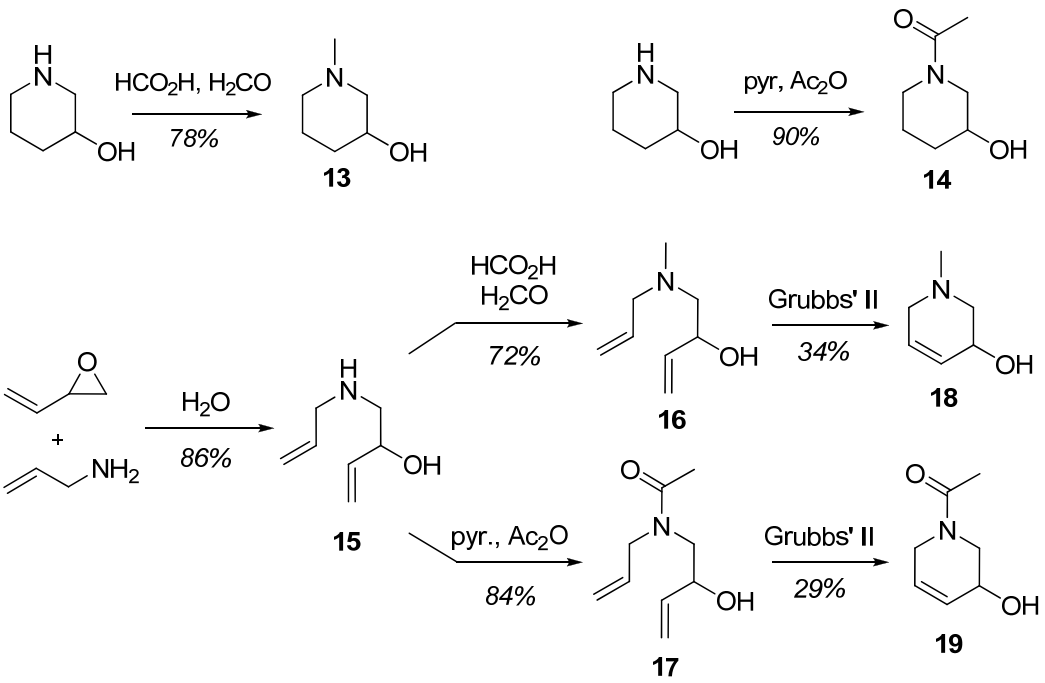

Scheme 6. Synthesis of nitrogen-containing sugar mimics.

Difficulties arose upon attempting to form the etheral linkage between the coumarin scaffold and various cyclohexanol derivatives. When coupling to noviose or other sugars, a Lewis acid-catalyzed procedure was utilized, however, when

coupling to derivatives that lacked the anomeric oxygen, this route did not provide any desired products. Additional efforts included tosylation and triflation of the alcohols, in hopes that the phenol could facilitate an SN2–type displacement under basic conditions. However, these were ineffective and produced only trace amounts of product, if any, perhaps due to the inefficient nucleophilicity of the phenolic oxygen.

We changed our strategy at this point to the esterification protocol developed by Mitsunobu *et. al.*[67] These procedures normally involve the use of triphenyl-phosphine (PPh_3) and a reactive azide species such as diethylazodi-carboxylate (DEAD). The triphenyl phosphine nucleophilically attacks the azo species, yielding a betaine intermediate species, which in turn deprotonates the phenol. The resulting ion deprotonates the alcohol, leaving the resultant alkoxide to form the critical oxophosphonium species and activating it as a leaving group, which is subsequently attacked by the phenolic anion to form the desired ether linkage (Scheme **7**).[68]

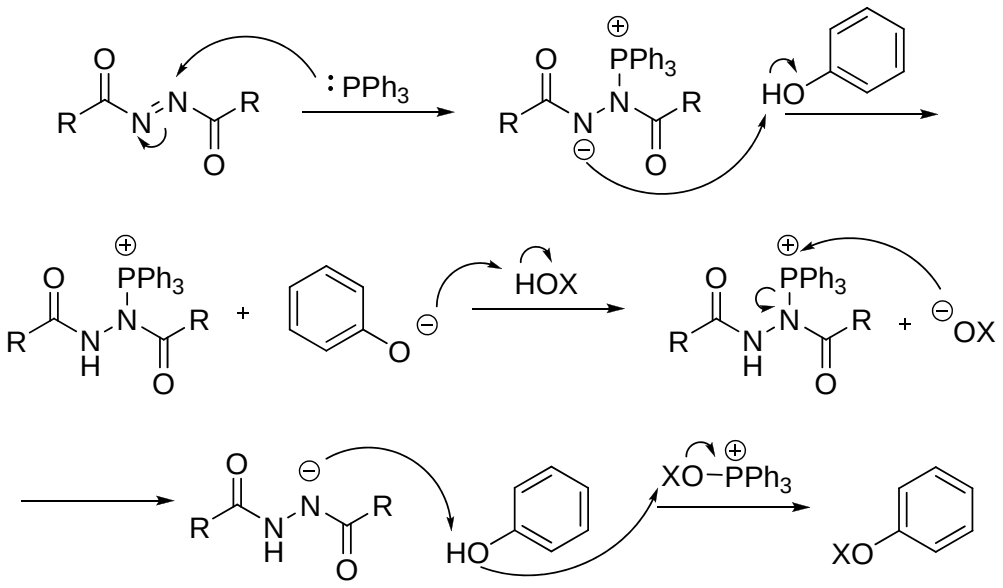

X = alkyl group
DEAD = diethylazodicarboxylate; R = OCH_2CH_3
DIAD = diisopropylazodicarboxylate; R = $OCH(CH_3)_2$
ADDP = 1,1'-(azodicarbonyl)dipiperidine; R = $N(CH_2)_5$

Scheme 7. Mechanism of the Mitsunobu esterification reaction and common reagents.

After initial attempts to couple the alcohols with the coumarin phenol moiety, it was proposed that the very low acidity of the phenol might prevent successful conversion. We therefore switched to the more reactive isopropyl derivative of DEAD, known as DIAD (diisopropylazodicarboxylate), and when these conditions also failed to yield the desired ether, an even more reactive species, 1,1'-(azodicarbonyl)dipiperidine (ADDP) was utilized (Scheme **7**). Though Mitsunobu esterification can often proceed in a one-pot fashion, it was necessary to first form the betaine intermediate, followed by addition of the alcohol and then the phenol. A

variety of temperatures and solvents were also tested in order to provide optimal conditions (Table **2**).

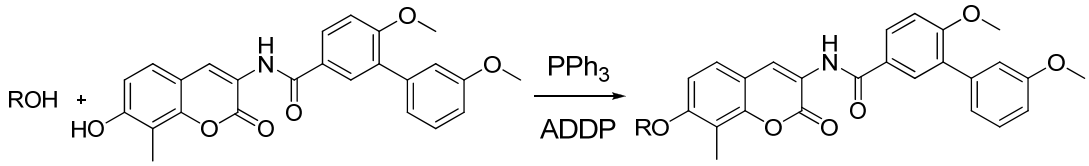

Solvent	Molar Equivalents			Temperature	Yield
	ROH	ArOH	PPh_3/ADDP		
CH_2Cl_2	1.0	1.0	1.5	0 - 25°C	--
	1.0	2.0	2.0	0 – 25°C	trace
	1.0	2.0	1.5	0 – 25°C	<5%
THF	1.0	1.0	1.5	0 - 25°C	trace
	2.0	1.0	1.5	0 – 25°C	trace
	1.0	2.0	1.5	0 – 25°C	8%
	1.0	2.0	1.3	0 – 25°C	35%
	1.0	2.0	1.3	25°C	42%
	1.0	2.0	1.3	50°C	22%
benzene	1.0	2.0	1.3	25°C	--
toluene	1.0	2.0	1.3	0 – 25°C	trace
	1.0	2.0	1.3	25°C	13%
	1.0	5.0	2.0	25°C	--

Table 1. Mitsunobu esterification conditions and results.

Although we did obtain products via these conditions, it was noted that the reactions proceeded much more efficiently when building each molecule separately, coupling each sugar mimic to the coumarin core before appending the benzamide side chain. Although this prevented us from taking advantage of common intermediates, it did result in improved overall yields for each of the three compounds, **22a-c**, as shown in Scheme **8**. However, this later-developed strategy is not able to be utilized for those compounds which undergo further dihydroxylation or subsequent

functionalization, due to the reductive side reactions that occur during the palladium-catalyzed hydrogenolysis used to cleave the Cbz group.

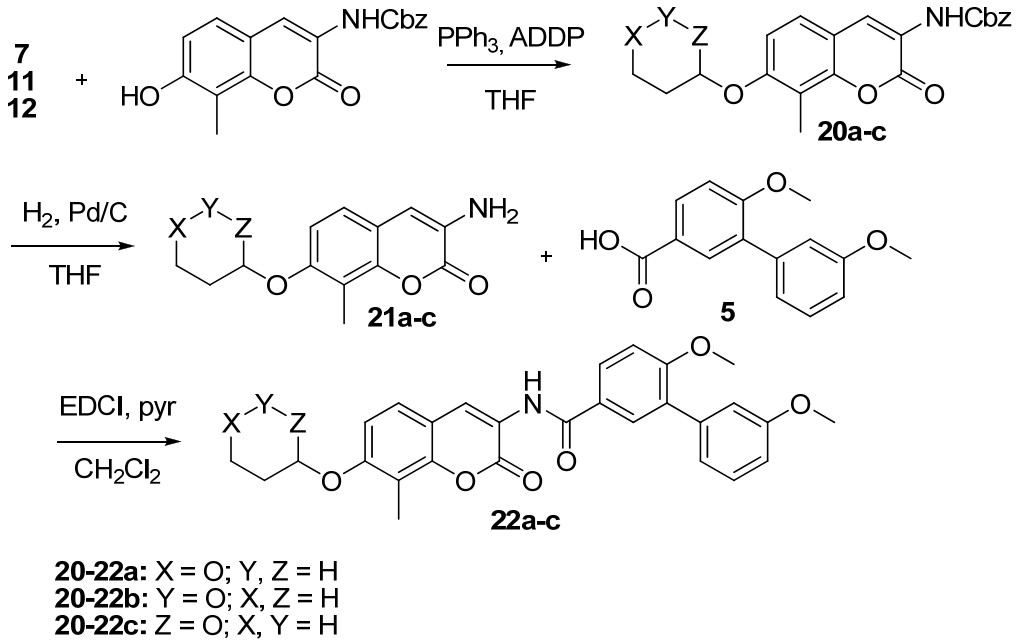

Scheme 8. Secondary route to access novobiocin analogues.

Further work to complete these final compounds, and others, for a full library of novobiocin derivatives containing sugar mimics is currently underway. Other ongoing efforts include the synthesis of five- and seven-membered sugar mimics, as well as cyclic alcohols with varying substituents about the ring, following previous work reported by the Blagg Laboratory. Future anti-proliferative assays and other biological studies will complete analyses of these analogues, which are hypothesized to show demonstrate improvements in selectivity and potency, as well as to provide

critical structure-activity relationships regarding the interaction of novobiocin derivatives with the Hsp90 *C*-terminus.

Computational studies. Structure-based drug design is frequently employed to design and evaluate potential inhibitors of the Hsp90 *N*-terminus in order to improve the efficiency of synthetic efforts. This is made possible by studying co-crystal structures of geldanamycin and radicicol within the *N*-terminal ATP-binding domain, removing the bound ligand and then using molecular docking programs to evaluate a ligand of choice. Comparisons of resultant binding energies, coupled with observations about relevant binding interactions within the pocket in question are used to determine which molecules demonstrate the highest affinity and, therefore, are worth synthesizing in the laboratory. In the absence of a co-crystal structure representing the Hsp90 *C*-terminus bound to an inhibitor, docking studies and comparisons present a significant challenge, as the correct conformation of the protein structure is based on similarity to other proteins or crystal structures alone.

Full-length crystal structures of Hsp90 reveal that the protein maintains an active dimer, exhibiting C2 symmetry.[69] Monomers of Hsp90 are known to be inactive;[69] it follows that inhibition of the dimerization domain would prevent the protein from assuming its active conformation and would lead to efficacious and selective Hsp90 inhibitors. The dimerization domain resides within the *C*-terminus of the protein, and contains four overlapping alpha-helices of various compositions. This is also proposed to be the site to which novobiocin and other *C*-terminal

inhibitors bind and inhibit the protein, although studies to date have been inconclusive and do not fit the structures provided by solution or crystal structures.

Several groups have proposed binding sites within the *C*-terminal domain, and suggest this region of the protein exists in both open and closed conformations, with inhibitors preventing dimerization.[60,70] However, available crystal structures do not exhibit an intact dimerization region with open nucleotide–binding motifs (Fig. **19**). Furthermore, none of the theoretical binding sites proposed to date match the biochemical results obtained for Hsp90.

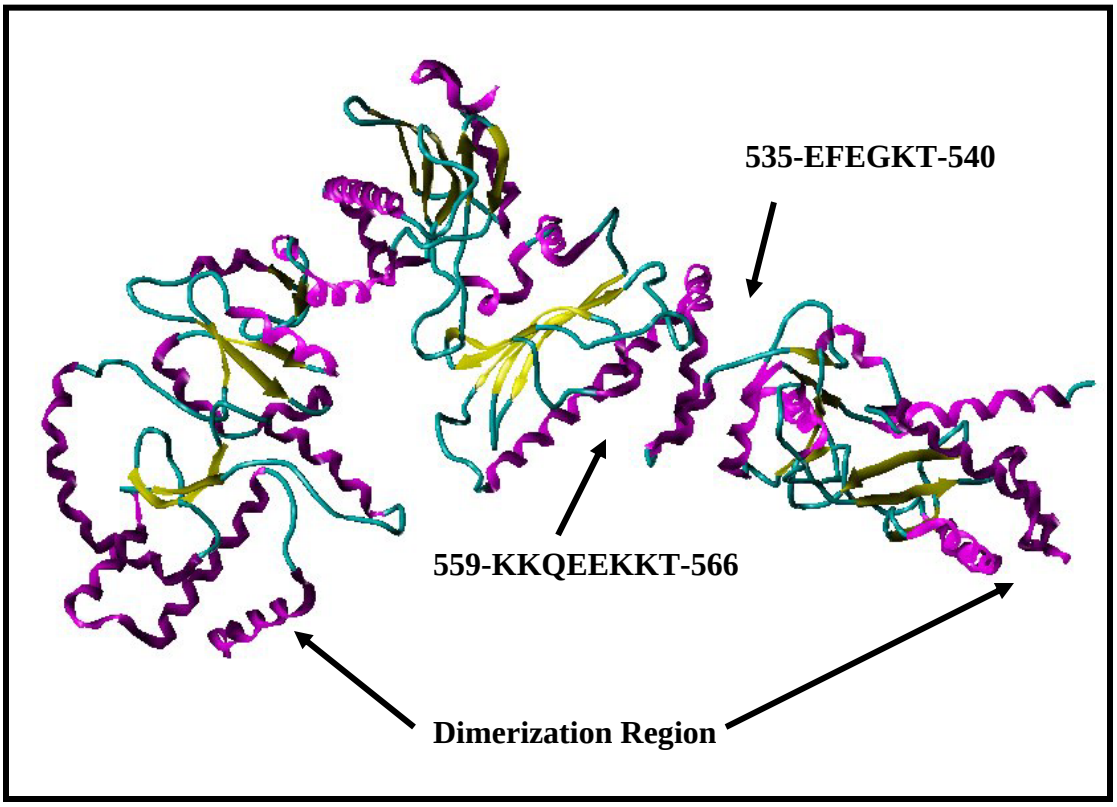

Figure 19. *C*-terminal crystal structure in open conformation with proposed binding sites **535-EFEGKT-540** and **559-KKQEEKKT-566**.

To alleviate this problem and to design a working model for the Hsp90 *C*-terminus to be used for computational predictions prior to synthetic efforts, the Blagg Laboratory produced four photolabile novobiocin analogues (Fig. **20**) to be used in photoaffinity studies in collaboration with the Matts Laboratory at Oklahoma State University.[71] After binding of these derivatives to Hsp90, they were irradiated with ultraviolet light to cleave the azide moiety, producing a reactive nitrene species, which underwent insertion into the *C*-terminal backbone. Following trypsin digests to cleave the protein at serine and threonine residues, the fragments were analyzed via mass spectrometry to determine the location at which the compounds inserted. These studies identified two previously unrecognized binding sites within the *C*-terminus, **535-EFEGKT-540** and **559-KKQEEKKT-566** (Fig. **19**), and provided new insights into the putative binding pocket.

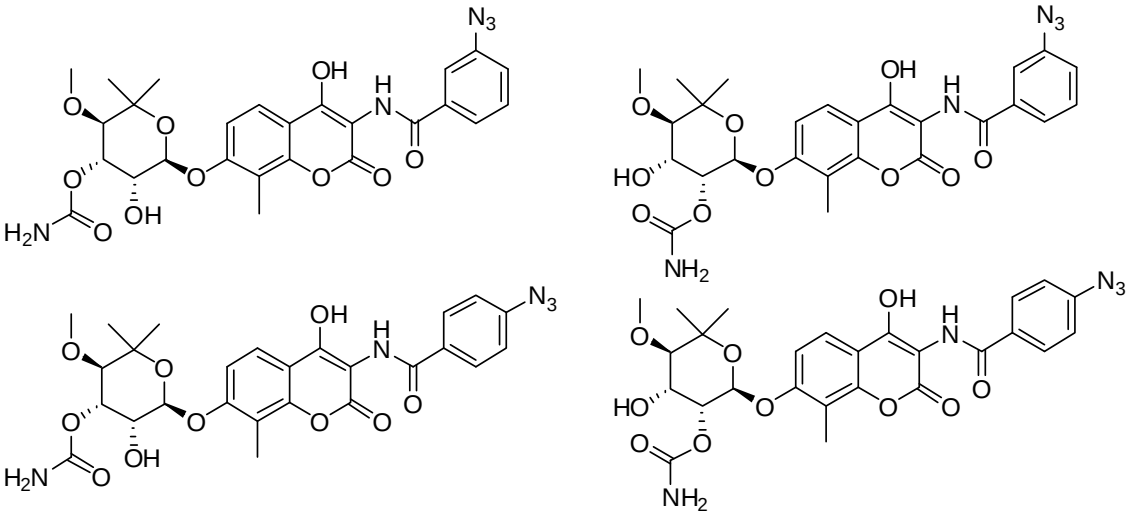

Figure 20. Photolabile novobiocin analogues.

Initial molecular docking studies with the only published *C*-terminal Hsp90 crystal structure, 2CGE, were performed in order to test the validity of this crystal structure for future structure-based design of analogues. A library of 100 ligands was generated using the Sybyl "Build" component, including 45were performed in order to test the validity of this crystal structure for future structure-based design of analogues. A library of 100 ligands was generated using the "build" component of the Sybyl software by Tripos, then analyzed via docking procedures within this framework. This series was designed with a broad range of structural variations and included natural products novobiocin, clorobiocin, derrubone, and coumermycin A1, along with derivatives of these compounds for which we had already obtained IC_{50} values in MCF-7 and SKBr3 cell lines.

Docking analyses were performed using the Autodock functionality, which provides approximations of the intermolecular energy interactions between the protein and ligand in kcals/mol, and can be used to determine potential binding sites and favorable conformations for the ligands of choice. Flexidock, another docking program used to supplement the information obtained, allows additional flexibility within the protein, which can be specified to the proposed active site. The algorithm-based Flexidock program also conducts calculations that account for electrostatic, torsional, and constraint energy terms to provide computational hypotheses for how each ligand may bind to the protein.

Results suggested the ligands bound randomly at sites unrecognized as critical regions within the 2CGE structure. Hypothesizing that the protein would exhibit

different conformations when binding *in vivo*, we set out to build new models that would exhibit a preferred conformation and provide pockets for ligand interaction. Using SwissModel and PyMol programs, which allow manipulation of the secondary and tertiary Hsp90 *C*-terminal and full-length protein structures, a series of four models was built **M1P-M4P**, each presenting different amino acids within the binding site in an attempt to optimize protein-ligand interactions (Fig. **21**).

Preliminary structure-activity relationships, based on the MCF-7 and SKBr3 cells antiproliferation values obtained experimentally, were used to predict which amino acid residues within the *C*-terminal domain might be critical for binding. This included manipulation of aromatic residues, such as Phe536, into the open pocket in an attempt to facilitate stacking interactions with the coumarin ring of our novobiocin analogues. **M1P** and **M4P** were both based on full-length Hsp90 crystal structure 2CG9, while **M2P** and **M3P** were modeled after 2CGE. These four models were converted into Sybyl Unix language format and hydrogen atoms were inserted to allow hydrogen-bonding capabilities.

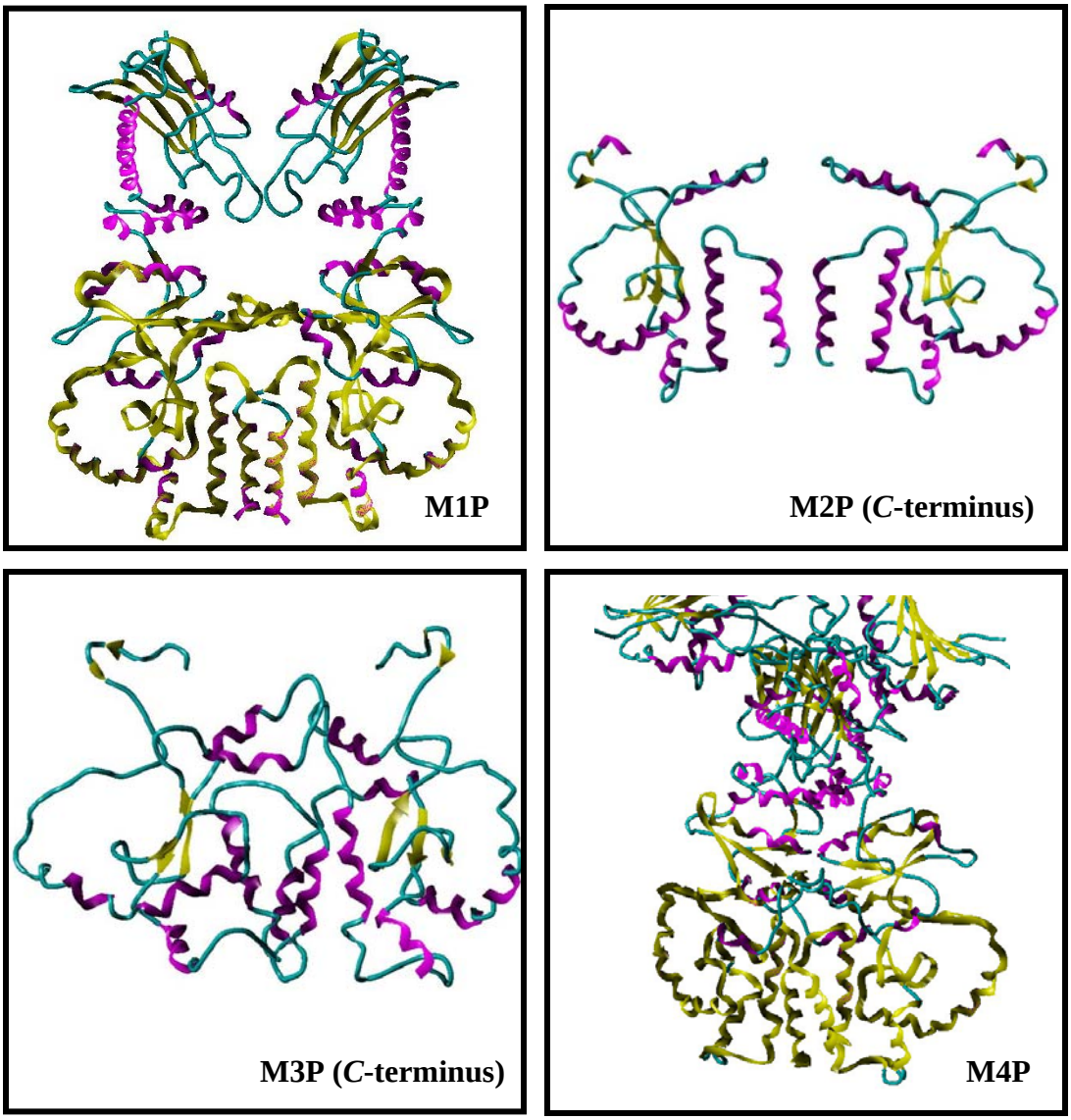

Figure 21. Ribbon diagrams of original model series **M1P-M4P**.

These four models were screened against the ligand library and evaluated for binding affinities. Preliminary investigation suggested that none of the analogues bound to sites identified via the photoaffinity binding studies. However, the best of these models, **M1P**, showed the ligands docked in an area proximal to an alternative

location (Fig. **22**). It was hypothesized that the flexibility of the protein might allow rotation upon binding to form interactions with the biochemically elucidated site.

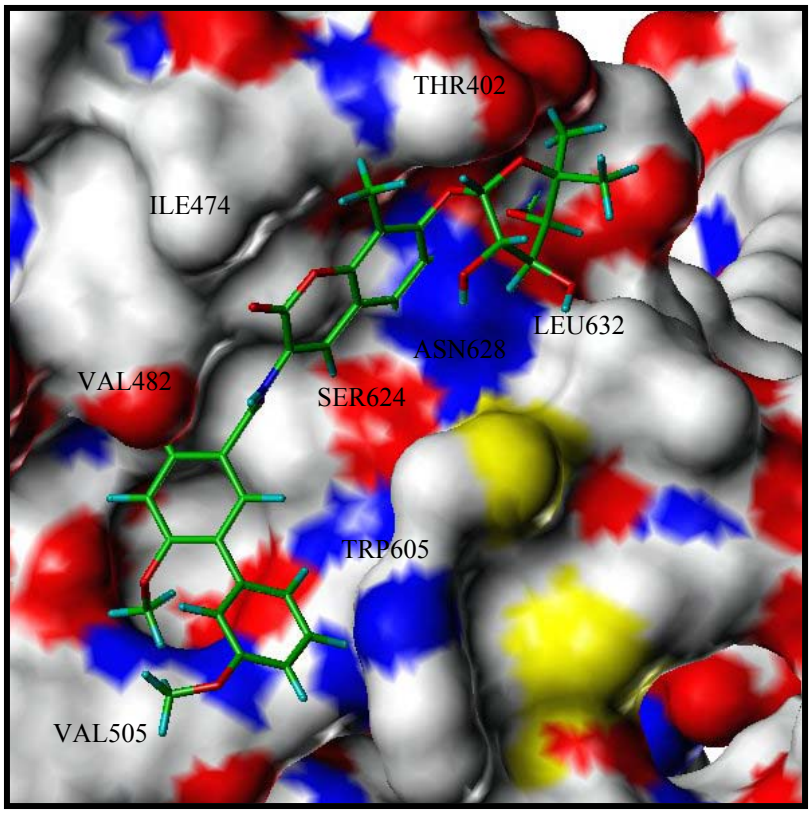

Figure 22. Novobiocin derivative KU-111 bound to model **M1P**.

Based on analyses of these docking studies, which include overlays of each ligand bound to its respective binding site, four new models, **1-4CT**, were designed using SwissModeler and PyMol. This set of structures was designed with the alpha helices of the dimerization domain in closer proximity to one another, based on our hypothesis that the ligands bind as the Hsp90 monomers approach their preferred conformation for dimerization. We also proposed that the monomers may rotate to a

greater degree than originally shown in the **M1P** model series, creating a pocket containing the **KKQEEKKT** domain, therefore the **CT** model series also accounted for this possibility while maintaining the C2 symmetry of the *C*-terminus (Fig. **23**).

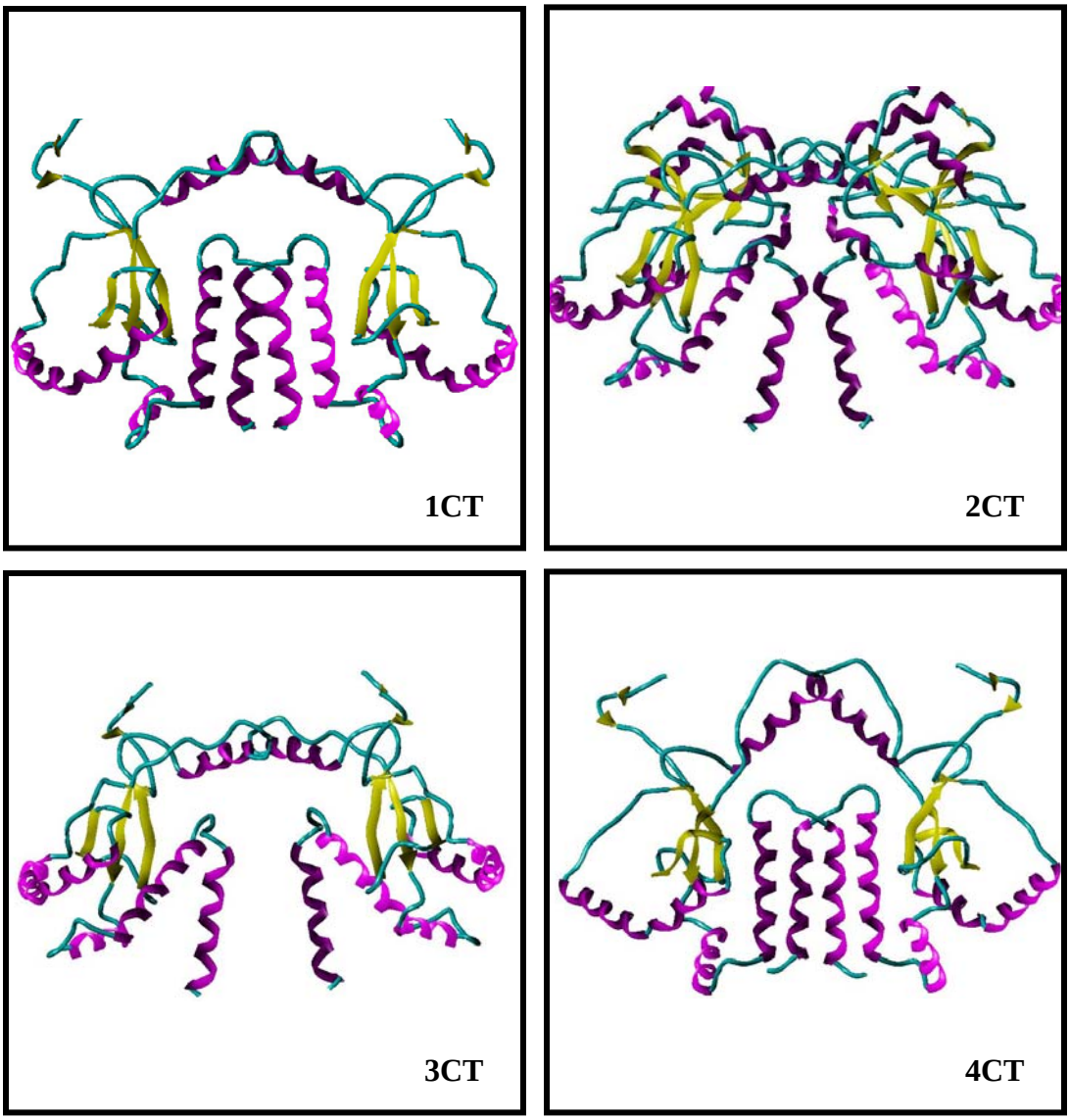

Figure 23. Second model series, **1-4CT**.

These models were converted into Sybyl format and evaluated using the Autodock and Flexidock molecular docking protocols. Model **3CT** was identified as the best in the series, based on the consistency of the binding results and the favorable enthalpic values produced upon docking. The overlapping alpha helices of the dimerization region exhibited by the **CT** series also allowed some of the dimeric coumermycin A1 analogues to dock simultaneously at similar regions on each of the two Hsp90 monomers. Although this data does not correspond to our experimental biochemical results, it provides useful information for further model design, indicating which residue conformations might allow or prevent accurate binding of the ligands within the *C*-terminal domain.

The **CT** studies showed consistent results with respect to docking location and orientation, as well as binding energies. The 100-ligand docking screen exhibited theoretical binding capabilities consistent with experimentally obtained *in vitro* data. For example, those compounds with the biaryl (KU-111B) or indole (KU-122) side chains were shown to have greater Hsp90-binding interactions (Fig. **24**) compared to the parent compound, which correlates with the improved IC_{50} values for these analogues. However, subsequent review demonstrated that the amino acids shown to be critical for binding in these computational studies, **670-ALLSSGFSL-678**, did not correlate with those identified via photoaffinity studies.

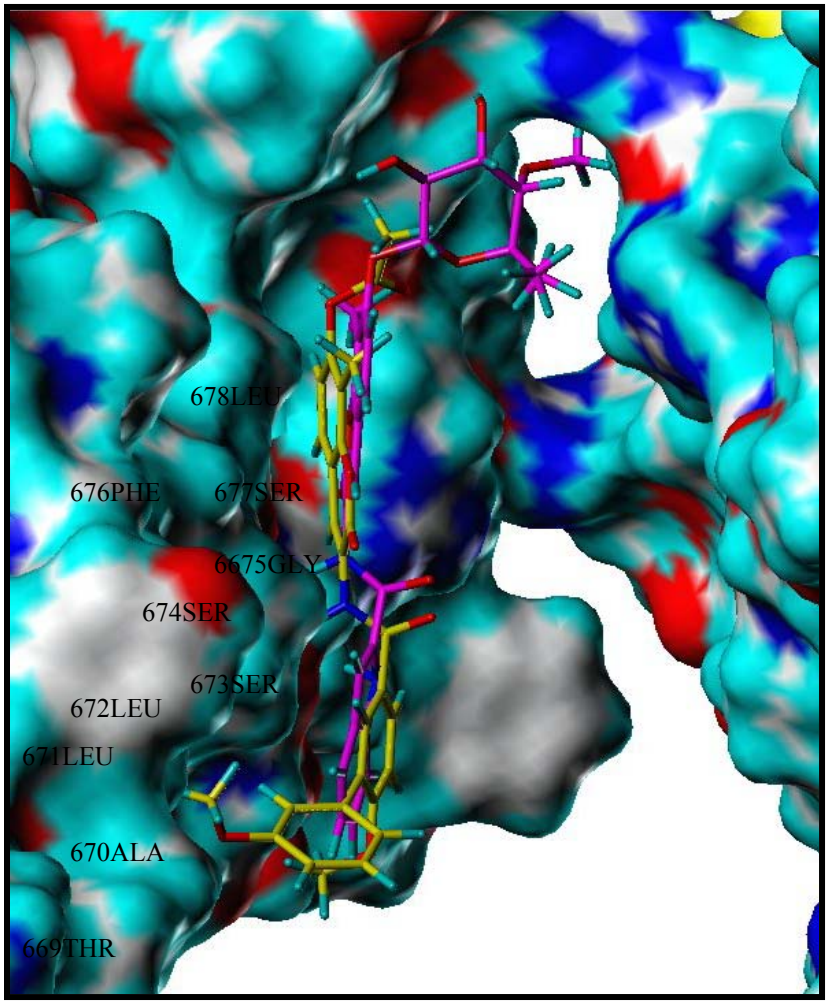

Figure 24. Analogues KU-111B and KU-122, docked to model **3CT.**

In early 2008, Bron *et. al.* published the first solution structures for apo-Hsp90, illustrating the vast magnitude of conformational changes of the Hsp90 protein and providing new insights toward the development of an accurate binding model of the C-terminus.[72] Based on these solution structures, we revised our earlier models, opening the bridge to the middle domain of Hsp90 and further rotating the *C*-

terminal monomers to produce three new models, **EM1-3** (Fig. **25**). These models showed more similarity with the published figures while also maintaining exposure to our identified binding sequences, **EFEGKT** and **KKQEEKKT**.

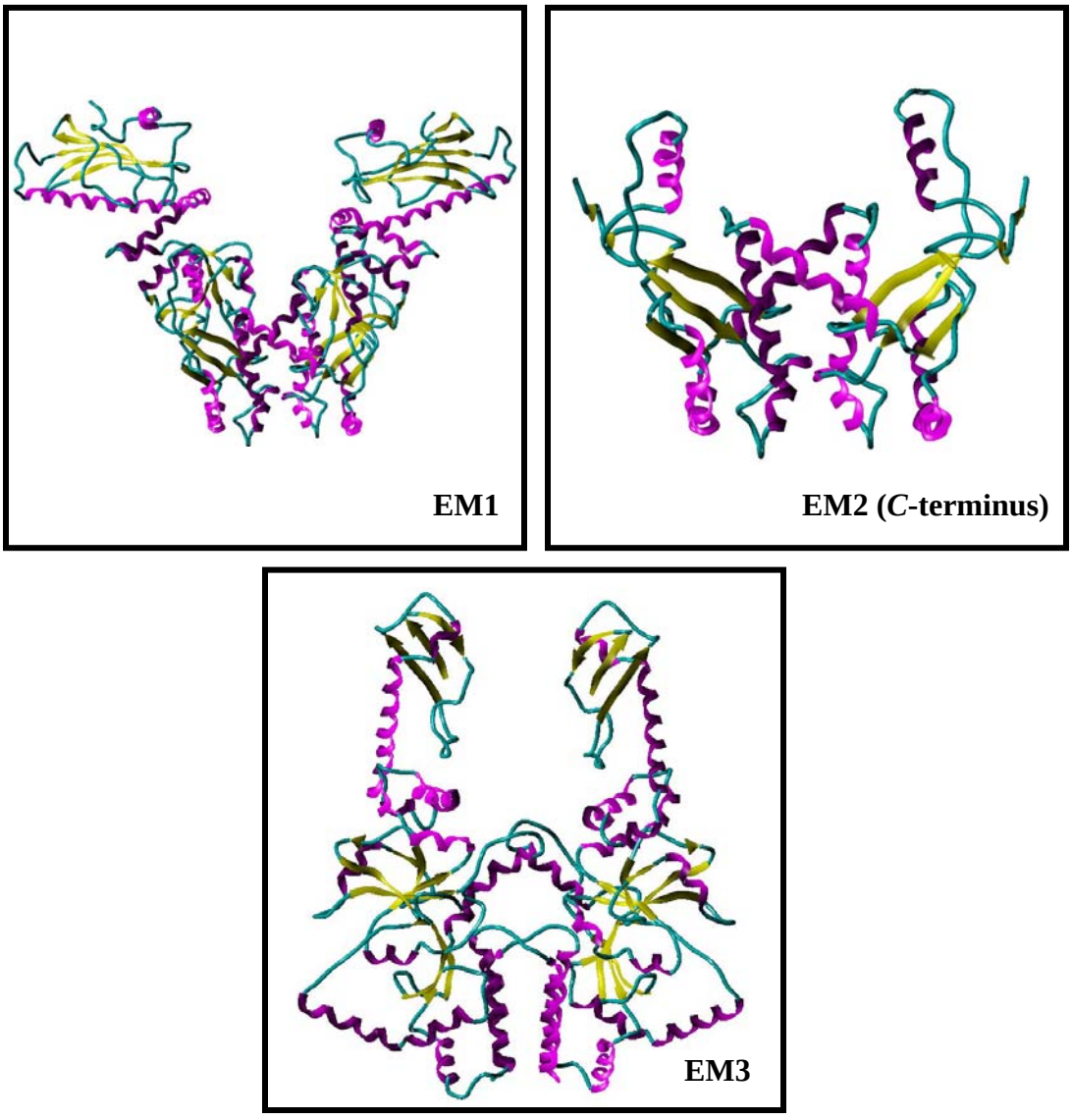

Figure 25. Model series **EM1-3**.

As before, we screened both full-length models (**EM1** and **EM3**) and one that included only the *C*-terminal residues (**EM2**) in an attempt to ensure that theoretical binding did not occur at other locations within the Hsp90 protein structure. Analyses of the docking results for the **EM** series showed ligands bound in an entirely different region, much closer to the middle domain than had been proposed by our previous computational models (Fig. **26**). Additionally, although these results exhibited some of the predicted ligand-amino acid interactions, the overall data still did not match the regions that had been identified via photoaffinity experiments. It was hypothesized that the very open structure of these models allowed the ligands to bind regions that would not be accessible *in vivo*, thus accounting for the inaccuracy of these results.

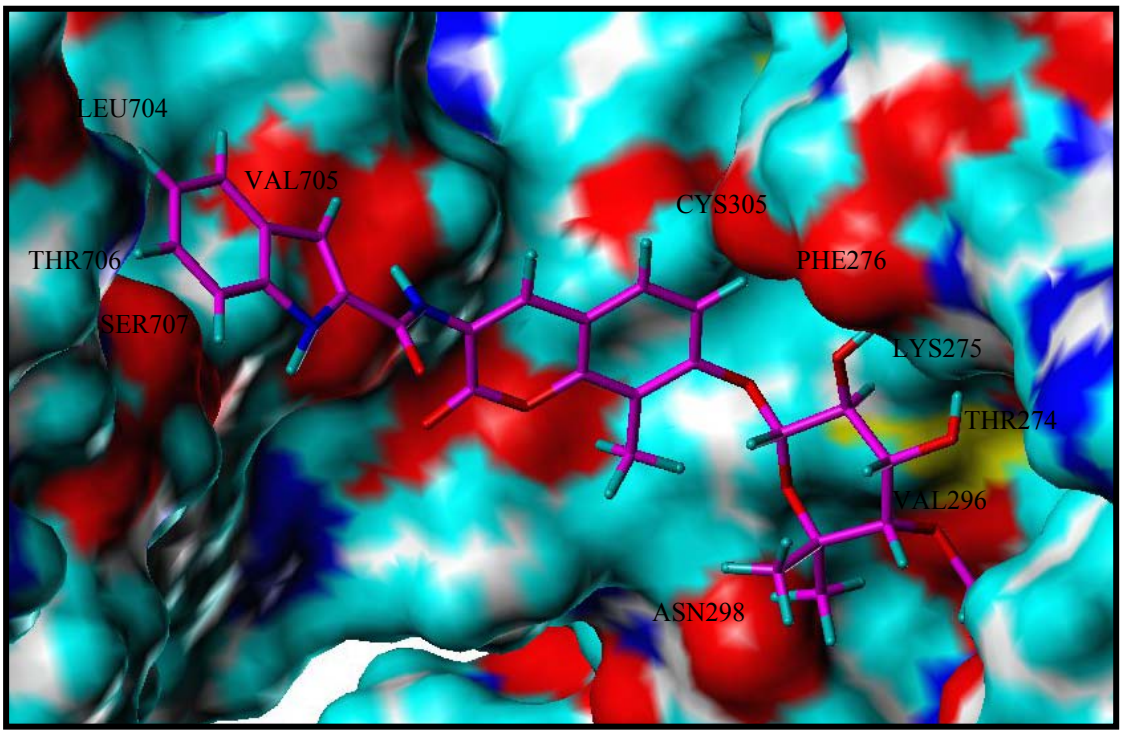

Figure 26. KU-122 bound to model **EM1**.

Overall, these results led us to conclude that the rigidity of both protein and ligand that is maintained in the Sybyl docking programs may prevent exposure of the ligand to the proper binding site. Addtionally, these docking algorithms do not bias the ligands to bind in a preferred site, and therefore other favorable interactions with the *C*-terminal backbone may interfere. Recent x-ray crystallography analyses of the *E. coli* Hsp90 homolog, htpG, by the Agard laboratory also provided new insight into the distinct conformations assumed by the protein in its open form, with no bound ligand, and in its closed form, after ATP or another ligand binds in the *N*-terminal domain.[73] This supplements earlier studies with geldanamycin and radicicol that show the *C*-terminal binding domain only becomes accessible after ATP or an inhibitor is bound to the *N*-terminus, suggesting that the dimerization domain of the protein undergoes radical conformational changes during this process.

Further studies involving the building of new models are currently underway, utilizing docking programs such as Surflex by Tripos, which allow for analysis specific to a proposed binding pocket. The InsightII Affinity package from Accelrys, Inc., has also shown promise, as this docking module includes dynamics simulations to overcome structural rigidity and to allow for protein movement close to the binding area. Comparative Molecular Field Analysis (CoMFA) studies are also in progress in hopes of obtaining useful *in silico* information for the prediction of efficacious new analogues of novobiocin and other C-terminal Hsp90 inhibitors.

Summary. This investigation has shown the continued synthetic efforts toward novel analogues of *C*-terminal Hsp90 inhibitor novobiocin. Structure-activity relationship studies of the coumarin and benzamide moieties of this molecule have yielded compounds with increased potency and may become clinical alternatives to *N*-terminal Hsp90 inhibitors. This study includes the design and synthesis of key derivatives of the noviose sugar, which will provide critical structure-activity relationship information upon biological evaluation. Additionally, this investigation has shown the design and analysis of numerous models of the Hsp90 *C*-terminus in an attempt to elucidate a model that can be used for future structure-based drug design. Continued synthetic and computational efforts in this area will lead to a better understanding of the interactions between Hsp90 and *C*-terminal inhibitors.

Experimental Data

General Methods. ^{1}H and ^{13}C NMR spectra were obtained on a Bruker DRX-400 instrument (400 MHz and 100.6 MHz, respectively). The samples were dissolved in $CDCl_3$. Chemical shifts are expressed in parts per million (δ) relative to the residual $CHCl_3$ serving as an internal standard. Abbreviations are as follows: s, singlet; d, doublet; t, triplet; q, quartet; m, multiplet; br, broad. Low resolution mass spectra (ES+, electrospray ionization, or FAB+, fast atom bombardment) were obtained using a Ribermag R10-10 quadrupole instrument. High resolution mass spectra (HRMS) were obtained using a VG Analytical ZAG double focusing spectrometer. All chromatographic separations were performed using Sorbent Technologies silica gel (230-400 mesh) or Analtech preparative layer TLC plates (250 or 1000 microns) with solvent mixtures as indicated. Benzene, dichloromethane, ether, tetrahydrofuran, and toluene (when used as reaction solvents) were purchased from Fisher Scientific and purified in a solvent purification system. All other solvents were purchased from Acros, Fisher Scientific, or Sigma-Aldrich and were used without further purification. All reactions that were not run in a reaction medium with water as a co-solvent were conducted in oven- or flame-dried reaction flasks that were cooled under argon. All reactions, unless otherwise specified, were performed in inert atmosphere under argon.

Materials. All reagents were purchased from Acros or Sigma-Aldrich chemical companies and used as received.

Experimental Section

The following compounds have been published by our laboratory: benzyl 7-hydroxy-8-methyl-2-oxo-*2H*-chromen-3-ylcarbamate (**1**),[63] 3-(benzyloxycarbonyl-amino)-8-methyl-2-oxo-*2H*-chromen-7-yl acetate (**2**),[63] 3-amino-8-methyl-2-oxo-*2H*-chromen-7-yl acetate (**3**),[63] methyl 3',6-dimethoxybiphenyl-3-carboxylate (**4**),[63] 3',6-dimethoxybiphenyl-3-carboxylic acid (**5**),[63] and *N*-(7-hydroxy-8-methyl-2-oxo-*2H*-chromen-3-yl)-3',6-dimethoxybiphenyl-3-carboxamide (**6**).[63]

The following compounds are known in the literature: cyclohex-2-enol (**9**),[74] tetrahydro-*2H*-pyran-3-ol (**10**),[75] tetrahydro-*2H*-pyran-2-ol (**11**),[76] tetrahydro-*2H*-pyran-4-ol (**12**),[76] and 1-methylpiperidin-3-ol (**13**).[77]

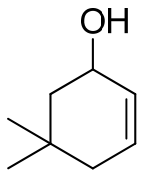

(7)

5,5-dimethylcyclohex-2-enol (7). Procedure adapted from literature.[78] 5,5-dimethylcyclohexan-2-dione (1.0 g, 7.2 mmol) was added slowly to a solution of $LiAlH_4$ (0.35 g, 9.2 mmol) in anhydrous Et_2O (40 mL) at reflux. The mixture was stirred at reflux for six hours, cooled to 0^oC, then quenched by dropwise addition of H_2O. The resulting suspension was extracted with Et_2O (3 x 50 mL). The combined organic layers were washed with water, brine, and dried (Na_2SO_4). The resulting oil

was purified via vacuum distillation to provide **7** as a colorless oil (0.49 g, 54%); (b.p. 68-70^{o}C).

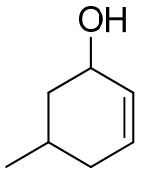

8

5-methylcyclohex-2-enol (8). Procedure adapted from literature.[78] 5-methyl cyclohexan-2-dione (1.0 g, 8.0 mmol) was added slowly to a solution of $LiAlH_4$ (0.39 g, 10 mmol) in anhydrous Et_2O (40 mL) at reflux. The mixture was stirred at reflux for six hours, cooled to 0^{o}C, and then quenched by dropwise addition of H_2O. The resulting suspension was extracted with Et_2O (3 x 50 mL). The combined organic layers were washed with water, brine, and dried (Na_2SO_4). The resulting oil was purified via vacuum distillation to provide **8** as a colorless oil (0.56 g, 62%); (b.p. 65-70^{o}C).

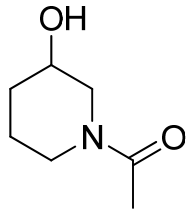

14

1-(3-hydroxypiperidin-1-yl)ethanone (14). 3-hydroxypiperidine (5.0 g, 49.5 mmol) was dissolved in a solution of pyridine (30 mL) and acetic anhydride (10 mL). The mixture was stirred overnight at rt. Solvent was removed in vacuo. The

resulting yellow solid was redissolved in EtOAc (10 mL) and diluted to 50 mL with H_2O, then extracted with EtOAc (3 x 50 mL). The combined organic layers were washed with brine, dried (Na_2SO_4), filtered, and concentrated to produce a yellow residue that was purified via column chromatography (5:1-2:1 hexanes:EtOAc) to provide **14** as a yellow amorphous solid (6.3 g, 90%); R_f = 0.48 (2:1 hexanes:EtOAc). ^{1}H NMR (400 MHz, $CDCl_3$) δ: 1.46 (m, 1H), 1.52 (m, 2H), 1.77 (m, 1H), 2.10 (s, 3H), 3.27 (m, 1H), 3.30 (br, 3H), 3.56 (m, 1H), 3.66 (br, 1H). ^{13}C NMR (100.6 MHz, $CDCl_3$) δ: 21.7, 23.5, 32.5, 49.4, 52.0, 70.0, 172.8. MS (FAB) *m/z* 143 (M^+1); HRMS (ES+) calcd for $C_7H_{13}NO_2Na$ (M^+Na): 166.0946, found 166.0950. IR (neat): 3420, 2950, 1670 cm^{-1}.

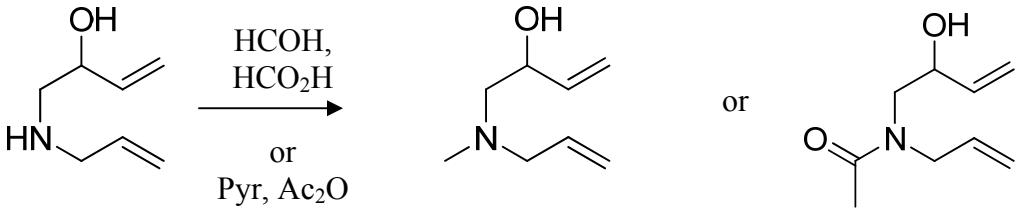

15 **16** **17**

1-(allylamino)but-3-en-2-ol (15), 1-(allyl(methyl)amino)but-3-en-2-ol (16), and *N*-allyl-*N*-(2-hydroxybut-3-enyl)acetamide (17) . To a solution of allylamine (20 mL, 47.1 mmol) and H_2O (1.2 mL, 66.0 mmol) at 0^{o}C was added butadiene monoxide (7.1 mL, 38.0 mmol) dropwise. The resulting mixture was stirred at reflux for 16 hours before cooling to rt and in vacuo to produce **15** as an off-white solid. The product was used as is without further purification.

(16): 1.0 g of **15** was dissolved in H_2O (5.0 mL). This solution was added dropwise to a stirring solution of 88% formic acid (4.4 mL, 96 mmol) and 37% formaldehyde (2.2 mL, 80 mmol) at 0°C under argon. The solution was warmed to rt and stirred for 1 hour before stirring at reflux overnight. After cooling to 0°C, a 50% aqueous NaOH solution was added to pH 9-10. Mixture was extracted with Et_2O (3 x 45 mL) and the combined organic layers were dried (Na_2SO_4), filtered, and concentrated in vacuo to produce a viscous yellow oil that was purified via column chromatography (5:1-1:1 hexanes:EtOAc) to provide **16** as a yellow oil (0.79 g, 72%); R_f = 0.84 (2:1 hexanes:EtOAc). ^{1}H NMR (400 MHz, $CDCl_3$) δ: 2.27 (s, 3H), 2.44 (m, 1H), 2.56 (m,1H), 2.96 (br, 1H), 3.11 (m, 2H), 4.25 (m, 1H), 5.16 (d, 1H), 5.22 (m, 2H), 5.39 (d, 1H), 5.83 (m, 2H). ^{13}C NMR (100.6 MHz, $CDCl_3$) δ: 43.0, 63.0, 65.7, 70.1, 115.8, 117.0, 134.3, 136.1. MS (ES+) *m/z* 142.1. (M^+1). IR (neat): 3390, 3010, 1370, 920, 890 cm^{-1}.

(17): 1.0 g of **15** was dissolved in a solution of pyridine (18 mL) and acetic anhydride (6 mL). The mixture stirred overnight at rt. The solvent was removed in vacuo, and the resulting yellow solid was redissolved in EtOAc (10 mL), diluted to 50 mL with H_2O, and extracted with EtOAc (3 x 50 mL). Combined organic layers were washed with brine, dried (Na_2SO_4), filtered, and concentrated to produce a yellow residue that was purified via column chromatography (5:1-2:1 hexanes:EtOAc) to provide **17** as a light yellow amorphous solid (1.12 g, 84%); R_f = 0.78 (2:1 hexanes:EtOAc). ^{1}H NMR (400 MHz, $CDCl_3$) δ: 2.30 (s, 3H), 3.12 (m, 1H), 3.41 (m, 1H), 3.78 (m, 1H), 4.44 (m, 1H), 5.20 (br. m, 3H), 5.39 (d, 1H), 5.82 (br. m, 2H). ^{13}C

NMR (100.6 MHz, $CDCl_3$) δ: 22.4, 44.4, 54.2, 78.3, 115.0, 116.3, 130.1, 136.0, 171.8. MS (ES+) *m/z* 170.1 (M^+1). IR (neat): 3350, 3100, 1640, 880, 860 cm^{-1}.

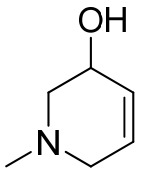

18

1-methyl-1,2,3,6-tetrahydropyridin-3-ol (18). To a solution of **16** (0.5 g, 3.5 mmol) dissolved in destabilized CH_2Cl_2 (10 mL) was added Grubbs' Second Generation Catalyst (0.17 g, 5 mol %) at rt. The reaction stirred at rt for 12 hours. The solution was then eluted through a plug of silica gel using a 40:1 solution of CH_2Cl_2 and acetone. The dark brown residue was purified via column chromatography (40:1 CH_2Cl_2:acetone) to afford 18 as an off-white solid (0.13 g, 34 %); R_f = 0.79 (40:1 CH_2Cl_2:acetone). ^1H NMR (400 MHz, $CDCl_3$) δ: 2.25 (s, 3H), 2.37 (m, 1H), 2.73 (m, 2H), 2.78 (m, 2H), 3.77 (m, 1H), 5.69 (m, 2H). ^{13}C NMR (100.6 MHz, $CDCl_3$) δ: 46.1, 56.0, 66.6, 71.0, 124.2, 128.1. MS (ES+) *m/z* 114.1 (M^+1); HRMS (ES+) calcd for $C_6H_{11}NONa$ (M^+Na): 136.0841, found 136.0843. IR (neat): 3420, 3080, 1240, 780 cm^{-1}.

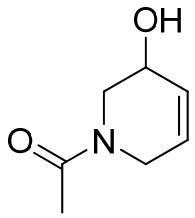

19

1-(5-hydroxy-5,6-dihydropyridin-1(*2H*)-yl)ethanone (19). To a solution of **17** (0.5 g, 3.0 mmol) dissolved in destabilized CH_2Cl_2 (10 mL) was added Grubbs' Second Generation Catalyst (0.12 g, 5 mol %) at rt. The reaction stirred at rt for 12 hours. The solution was then eluted through a plug of silica gel using a 40:1 solution of CH_2Cl_2 and acetone. The dark brown residue was purified via column chromatography (40:1 CH_2Cl_2:acetone) to afford **19** as a light yellow amorphous solid (0.12 g, 29%); R_f = 0.70 (40:1 CH_2Cl_2:acetone). ^{1}H NMR (400 MHz, $CDCl_3$) δ: 2.33 (s, 3H), 3.49 (m, 1H), 3.76 (m, 1H), 3.92 (br. m, 3H), 5.70 (m, 1H), 5.75 (m, 1H). ^{13}C NMR (100.6 MHz, $CDCl_3$) δ: 22.5, 44.0, 59.6, 70.8, 124.8, 127.9, 170.0. MS (ES+) *m/z* 141.1 (M^+1); HRMS (ES+) calcd for $C_6H_{11}NONa$ (M^+Na): 164.0790, found 164.0791. IR (neat): 3410, 3100, 1630, 1570, 820 cm^{-1}.

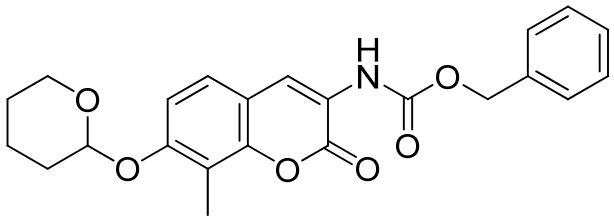

20a

Benzyl 8-methyl-2-oxo-7-(tetrahydro-*2H*-pyran-2-yloxy)-*2H*-chromen-3-ylcarbamate (20a). Triphenylphosphine (0.20 g, 0.76 mmol) was dissolved in anhydrous THF (5 mL) at rt. A solution of ADDP (0.19 g, 0.76 mmol) in THF (1 mL) was added dropwise to the PPh_3 solution. The mixture stirred for ten minutes before adding alcohol **11** (0.056 g, 0.55 mmol) dropwise. The resulting mixture stirred an additional ten minutes, then phenol **1** (0.4 g, 1.2 mmol) was dissolved in 4 mL THF and cannulated into the solution. The reaction stirred overnight at rt. The resulting mixture was concentrated via a stream of argon and the residue purified via column chromatography (10:1-2:1 hexanes:EtOAc) to afford **20a** as a yellow solid (0.095 g, 41%); R_f = 0.43 (2:1 hexanes:EtOAc). ^{1}H NMR (400 MHz, $CDCl_3$) δ: 1.58 (m, 2H), 1.68 (m, 2H), 1.89 (m, 1H), 2.07 (m,1H), 2.23 (s, 3H), 3.46 (m,1H), 3.53 (m,1H), 5.25 (s, 2H), 5.71 (m, 1H), 7.16 (d, 1H), 7.35-7.49 (br. m, 7H), 8.27 (s, 1H). ^{13}C NMR (100.6 MHz, $CDCl_3$) δ: 9.9, 19.8, 25.7, 31.8, 64.0, 64.8, 104.1, 110.2, 112.9, 118.9, 120.8, 126.4, 127.0, 128.0, 129.2, 135.5, 150.1, 150.8, 152.9, 156.7, 160.0. MS (ES+) *m/z* 410.2 (M^+1); HRMS (ES+) calcd for $C_{23}H_{24}NO_6$ (M^+1): 410.1525, found 410.1528. IR (neat): 2920, 1730, 1640, 1400, 1380, 1110, 840, 680 cm^{-1}.

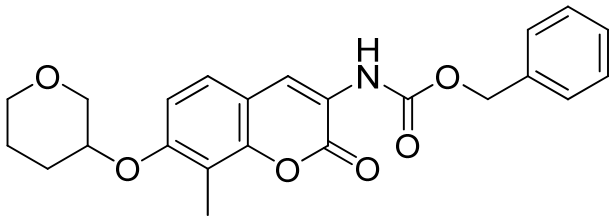

20b

Benzyl 8-methyl-2-oxo-7-(tetrahdro-*2H*-pyran-3-yloxy)-*2H*-chrome-3-yl-carbamate (20b). Followed general procedure to make **20a**, using alcohol **10** (0.056 g, 0.55 mmol). The resulting mixture was concentrated via a stream of argon and the residue purified via column chromatography (10:1-2:1 hexanes:EtOAc) to afford **20b** as a light yellow solid (0.054 g, 24%); R_f = 0.40 (2:1 hexanes:EtOAc). ^{1}H NMR (400 MHz, $CDCl_3$) δ: 1.61 (m, 2H), 1.72 (m, 2H), 2.07 (m, 1H), 2.37 (s, 3H), 3.83 (m, 1H), 3.89 (m, 2H), 5.24 (2H), 7.13 (d, 1H), 7.26 (s, 1H), 7.38-7.43 (br. m, 7 H), 8.28 (s, 1H). ^{13}C NMR (100.6 MHz, $CDCl_3$) δ: 10.1, 25.6, 30.2, 66.7, 69.6, 76.0, 79.1, 111.2, 112.9, 118.9, 121.2, 126.4, 127.4, 128.2, 136.5, 150.3, 154.1. MS (ES+) *m/z* 410.2 (M^+1); HRMS (ES+) calcd for $C_{23}H_{24}NO_6$ (M^+1): 410.1525, found 410.1526 IR spectral data not available for this compound.

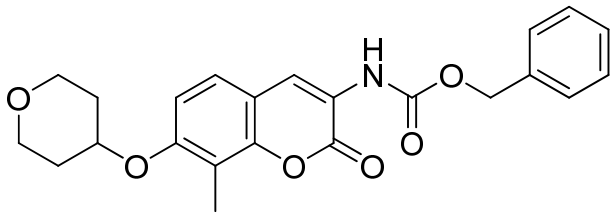

20c

Benzyl 8-methyl-2-oxo-7-(tetrahdro-*2H*-pyran-4-yloxy)-*2H*-chromen-3-yl-carbamate (20c). Followed general procedure to make **20a**, using alcohol **12** (0.056 g, 0.55 mmol). The resulting mixture was concentrated via a stream of argon and the residue purified via column chromatography (10:1-2:1 hexanes:EtOAc) to afford **20c** as a light yellow solid (0.043 g, 19%); R_f = 0.40 (2:1 hexanes:EtOAc). ^{1}H NMR (400 MHz, $CDCl_3$) δ: 1.79 (m, 2H), 2.11 (m, 2H), 2.23 (s, 3H), 3.64 (m, 2H), 3.75 (m, 2H), 3.89 (m, 1H), 5.16 (s, 2H), 6.85 (d, 1H), 7.32-7.58 (br. m, 7H), 8.26 (s, 1H). ^{13}C NMR (100.6 MHz, $CDCl_3$) δ: 10.0, 35.2, 62.6, 62.8, 66.7, 76.0, 111.8, 114.0, 118.6, 120.0, 126.7, 127.0, 127.4, 128.2, 128.6, 135.9, 151.1, 151.7, 154.6, 155.9, 160.1. MS (ES+) *m/z* 410.2 (M^+1); HRMS (ES+) calcd for $C_{23}H_{24}NO_6$ (M^+1): 410.1525, found 410.1524. IR (neat): 2860, 1710, 1650, 1630, 1450, 1210, 1050, 1020, 870, 710 cm^{-1}.

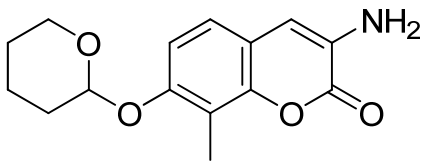

21a

3-amino-8-methyl-7-(tetrahydro-*2H*-pyran-2-yloxy)-*2H*-chromen-2-one (21a). **20a** (0.02 g, 0.049 mmol) was dissolved in THF (7 mL) at rt. 10% Pd/C (0.005 g, 10 mol %) was added at once. The flask was flushed with argon (2x) and H_2 (2x) before allowing to stir at rt under H_2 atmosphere overnight. The flask was again flushed with argon, then the resulting mixture was eluted through a one-inch

plug of silica gel (1:1 hexanes:EtOAc). The collected solvent was concentrated via a stream of air to afford **21a** as an off-white solid (0.013 g, quant. yield); R_f = 0.24 (2:1 hexanes:EtOAc). ^{1}H NMR (400 MHz, $CDCl_3$) δ: 1.57 (m, 2H), 1.69 (m, 2H), 1.91 (m, 1H), 2.07 (m, 1H), 2.38 (s, 3H), 3.62 (m, 2H), 4.07 (br, 2H), 5.49 (m, 1H), 6.72 (s, 1H), 6.98 (d, 1H), 7.38 (d, 1H). ^{13}C NMR (100.6 MHz, $CDCl_3$) δ: 9.9, 21.2, 25.8, 31.0, 63.0, 103.5, 111.1, 114.2, 114.6, 121.0, 126.4, 138.3, 151.0, 157.8, 161.1. MS (ES+) *m/z* 276.1 (M^+1). IR (neat): 3290, 2880, 1670, 1380, 1340, 700, 670 cm^{-1}.

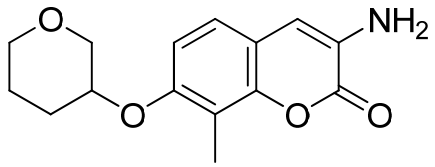

21b

3-amino-8-methyl-7-(tetrahydro-*2H*-pyran-3-yloxy)-*2H*-chromen-2-one (21b). Followed general procedure to make **21a**, starting from **20b** (0.02 g, 0.049 mmol). After stirring overnight, the resulting mixture was eluted through a one-inch plug of silica gel (1:1 hexanes:EtOAc). The collected solvent was concentrated via a stream of air to afford **21b** as an off-white solid (0.013 g, quant. yield); R_f = 0.22 (2:1 hexanes:EtOAc). ^{1}H NMR (400 MHz, $CDCl_3$) δ: 1.58 (m, 2H), 1.90 (m, 1H), 2.10 (m, 1H), 2.30 (s, 3H), 3.58 (m, 2H), 3.91 (m, 2H), 4.14 (m, 1H), 4.56 (br. s, 2H), 7.01 (s, 1H), 7.22 (d, 1H), 7.38 (d, 1H). ^{13}C NMR (100.6 MHz, $CDCl_3$) δ: 9.9, 23.9, 29.2, 69.8, 74.5, 77.9, 111.2, 113.7, 114.1, 120.0, 126.6, 138.2, 151.1, 158.2, 161.4. MS

(ES+) *m/z* 276.2 (M^+1). IR (neat): 3310, 2880, 1660, 1350, 1290, 1160, 910, 820, 750 cm^{-1}.

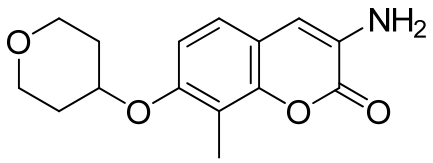

21c

3-amino-8-methyl-7-(tetrahydro-*2H*-pyran-4-yloxy)-*2H*-chromen-2-one (21c). Followed general procedure to make **21a**, starting from **20c** (0.20 g, 0.49 mmol). After stirring overnight, the resulting mixture was eluted through a one-inch plug of silica gel (1:1 hexanes:EtOAc). The collected solvent was concentrated via a stream of air to afford **21c** as an off-white solid (0.012 g, 90%); R_f = 0.24 (2:1 hexanes:EtOAc). ^1H NMR (400 MHz, $CDCl_3$) δ: 1.80 (m, 2H), 2.07, (m, 2H), 2.23 (s, 3H), 3.61 (br. m, 4H), 4.01 (m, 1H), 4.44 (s, 2H), 6.89 (s, 1H), 7.18 (d, 1H), 7.45 (d, 1H). ^{13}C NMR (100.6 MHz, $CDCl_3$) δ: 10.0, 35.1, 63.7, 75.8, 111.2, 112.8, 113.2, 120.0, 126.5, 137.9, 151.8, 157.6, 160.2. MS (ES+) *m/z* 276.1 (M^+1). IR spectral data not available for this compound.

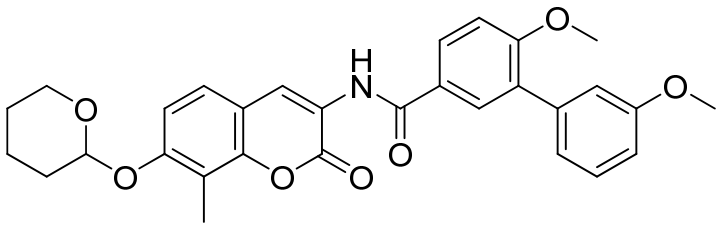

22a

3',6-dimethoxy-*N*-(8-methyl-2-oxo-7-(tetrahydro-*2H*-pyran-2-yloxy)-*2H*-chromen-3-yl)biphenyl-3-carboxamide (22a). Amine **21a** (0.013 g, 0.049 mmol) was dissolved in CH_2Cl_2 (3 mL) at rt. Next, biaryl acid **5** (0.025 g, 0.098 mmol) was added in one step. To this stirring solution was added EDCI (0.024 g, 0.123 mmol), followed by pyridine (1.5 mL). The resulting mixture stirred at rt for 18 hours under argon. The solution was concentrated via a stream of air and purified via preparative chromatography (40:1 CH_2Cl_2: acetone) to afford **22a** as a white solid (0.010 g, 38 %); R_f = 0.77 (40:1 CH_2Cl_2: acetone). ^{1}H NMR (400 MHz, $CDCl_3$) δ: 1.64 (m, 2H), 1.71 (m, 2H), 1.91 (m, 1H), 2.09 (m, 1H), 2.27 (s, 3H), 3.73 (m, 2H), 3.91 (s, 3H), 3.95 (s, 3H), 5.66 (m, 1H), 7.03 (d, 1H), 7.29-7.57 (m, 8H), 8.12 (s, 1H), 8.63 (d, 1H). ^{13}C NMR (100.6 MHz, $CDCl_3$) δ: 10.1, 21.0, 25.1, 31.0, 55.8, 56.1, 62.0, 104.9, 110.9, 111.3, 113.5, 113.8, 117.6, 120.2, 122.9, 125.9, 126.1, 128.0, 128.6, 130.1, 130.4, 136.7, 138.3, 153.9, 155.5, 160.0, 163.1, 168.9. MS (ES+) *m/z* 516.2 (M^+1); HRMS (ES+) calcd for $C_{30}H_{29}NO_7Na$ (M^+Na): 538.1944, found 538.1946. IR (neat): 3030, 2860, 1720, 1630, 1390, 1300, 1090, 870, 770 cm^{-1}.

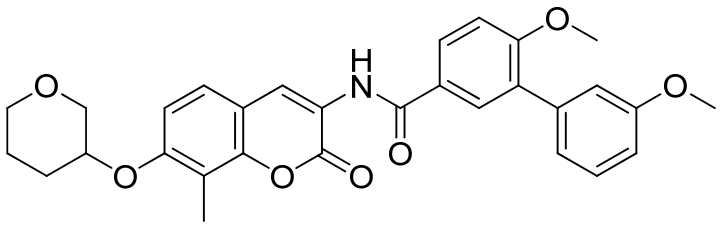

22b

3',6-dimethoxy-*N*-(8-methyl-2-oxo-7-(tetrahydro-*2H*-pyran-3-yloxy)-*2H*-chromen-3-yl)biphenyl-3-carboxamide (22b). Followed general procedure to make **22a**, starting from **21b** (0.013 g, 0.049 mmol). The resulting solution was concentrated via a stream of air and purified via preparative chromatography (40:1 CH_2Cl_2: acetone) to afford **22b** as an off-white solid (0.006 g, 22 %); R_f = 0.68 (40:1 CH_2Cl_2: acetone). ^{1}H NMR (400 MHz, $CDCl_3$) δ: 1.58 (m, 2H), 1.90 (m, 1H), 2.10 (m, 1H), 2.30 (s, 3H), 3.58 (m, 2H), 3.91 (m, 2H), 3.96 (s, 3H), 4.01 (s, 3H), 4.14 (m, 1H), 6.99 (d, 1H), 7.29-7.41 (br. m, 8H), 8.12 (s, 1H), 8.55 (s, 1H). ^{13}C NMR (100.6 MHz, $CDCl_3$) δ: 9.6, 24.9, 30.0, 54.5, 55.1, 69.8, 76.2, 79.7, 110.8, 111.1, 114.4, 118.9, 119.6, 121.1, 124.0, 125.5, 126.2, 126.4, 129.9, 132.2, 136.8, 137.1, 152.7, 153.8, 159.4, 160.3, 169.0. MS (ES+) *m/z* 516.2 (M^+1). IR (neat): 2990, 2840, 1710, 1450, 920, 780 cm^{-1}.

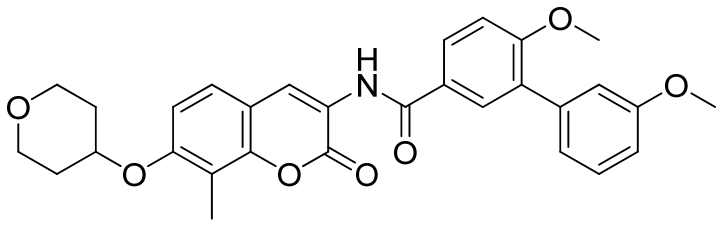

22c

3',6-dimethoxy-*N*-(8-methyl-2-oxo-7-(tetrahydro-*2H*-pyran-4-yloxy)-*2H*-chromen-3-yl)biphenyl-3-carboxamide (22c). Followed general procedure to make **22a**, starting from **21c** (0.012 g, 0.043 mmol). The resulting solution was concentrated via a stream of air and purified via preparative chromatography (40:1 CH_2Cl_2: acetone) to afford **22c** as an off-white solid (0.006 g, 28%); R_f = 0.73 (40:1 CH_2Cl_2: acetone). ^{1}H NMR (400 MHz, $CDCl_3$) δ: 1.81 (m, 2H), 2.09, (m, 2H), 2.21 (s, 3H), 3.60 (br. m, 4H), 3.86 (s, 3H), 3.89 (s, 3H), 3.94 (m, 1H), 6.98 (d, 1H), 7.30-7.49 (br. m, 8H), 8.18 (s, 1H), 8.45 (s, 1H). ^{13}C NMR (100.6 MHz, $CDCl_3$) δ: 9.9, 26.2, 30.0, 56.2, 57.8, 71.0, 73.7, 78.9, 109.5, 111.3, 112.6, 113.4, 119.1, 120.2, 120.9, 126.2, 126.5, 127.3, 127.8, 129.9, 132.5, 137.4, 139.2, 150.1, 156.2, 158.3, 160.1, 160.4, 168.1. MS (ES+) *m/z* 516.1 (M^+1); HRMS (ES+) calcd for $C_{30}H_{29}NO_7Na$ (M^+Na): 538.1944, found 538.1939. IR (neat): 2860, 2800, 1730, 1640, 1500, 1440, 1230, 920, 890, 810 cm^{-1}.

References

1) Hanahan, D.; Weinberg, R. A. *Cell* **2000**, *100*, 57-70.

2) DeBoer, C.; Meulman, P.A.; Wnuk, R.J.; Peterson, D.H. *J. Antibiot.* **1970**, *23*, 442-447.

3) Jove, R.; Hanafusa, H. *Annu. Rev. Cell. Bio.* **1987**, *3*, 31–56.

4) Uehara, Y.; Murakami, Y.; Mizuno, S.; Kawai, S. *Virology* **1988**, *164*, 294–298.

5) Whitesell, L.; Shifrin, S.D.; Schwab, G.; Neckers, L.M. *Cancer Res*. ***1992***, *52*, 1721–1728.

6) Whitesell, L.; Mimnaugh, E.G.; De Costa, B.; Myers, C.E.; Neckers, L.M. *Proc. Natl. Acad. Sci.* **1994**, *91*, 8324-8328.

7) Eleuteri, A.M.; Cuccioloni, M.; Bellesi, J.; Lupidi, G.; Fioretti, E.; Angeletti, M. *Proteins: Struc. Funct. Genet.* **2002**, *48*, 169–177.

8) Stebbins, C.E.; Russo, A.A.; Schneider, C.; Rosen, N.; Hartl, F.U.; Pavletich, N.P. *Cell* **1997**, *89*, 239-250.

9) Prodromou, C.; Roe, S.M.; O'Brien, R.; Ladbury, J.E.; Piper, P.W.; Pearl L.H. *Cell* **1997**, *90*, 65-75.

10) Schnur, R.C.; Corman, M.L. *J. Org. Chem.* **1994**, *59*, 2581-2584.

11) Rinehart, K.L.; Shield, L.S. *Fortschr. Chem. Org. Naturst.* **1976**; *33*, 231–307.

12) Roe, M.S.; Prodromou, C.; O'Brien, R.; Ladbury, J.E.; Piper, P.W.; Pearl, L.H. *J. Med. Chem.* **1999**, *42*, 260-266.

13) Dikalov, S.; Landmesser, U.; Harrison, D.G. *J. Biol. Chem.* **2002**, *277*, 25480–25485.

14) Supko, J.G.; Hickman, R.L.; Grever, M.R.; Malspeis, L. *Cancer*. *Chemother. Pharmacol.* **1995**, *36*, 305–315.

15) Schnur, R.C.; Corman, M.L.; Gallaschum, R.J.; Cooper, B.A.; Dee, M.F.; Doty, J.L.; Muzzi, M.L.; Moyer, J.D.; DiOrio, C.I.; Barbacci, E.G.; Miller,

P.E.; O'Brien, A.T.; Morin, M.J.; Foster, B.A.; Pollack, V.A., Savage, D.M.; Sloan, D.E.; Pustilnik, L.R.; Moyer, M.P. *J. Med. Chem.* **1995**, *38*, 3806-3812.

16) Schulte, T.W.; Neckers, L.M. *Cancer Chemother. Pharmacol.* **1998**, *42*, 273–279.

17) Banerji, U. *Proc. Am. Assoc. Cancer. Res*. **2003**, *44*, 677.

18) Sausville, E.A. *Curr. Cancer Drug Targets* **2003**, *3*, 377–383.

19) Tian, Z-Q.; Liu, Y.; Zhang, D.; Wang, Z.; Dong, S.D.; Carreras, C.W.; Zhou, Y.; Rastelli, G.; Santi, D.V.; Myles, D.C. *Bioorg. Med. Chem.* **2004**, *12*, 5317-5329.

20) Jez, J.M.; Chen, J.C–H.; Rastelli, G.; Stroud, R.M.; Santi, D.V. *Chem. Biol.* **2003**, *10*, 361–368.

21) Zheng, F.F.; Kuduk, S.D.; Chiosis, G.; Munster, P.N.; Sepp-Lorenzino, L.; Danishefsky, S.J.; Rosen, N. *Cancer Res.* **2000**, *60*, 2090-2094.

22) Kuduk, S.D.; Zheng, F.F.; Sepp-Lorenzino, L.; Rosen, N.; Danishefsky, S.J. *Bioorg. Med. Chem. Lett.* **1999**, *9*, 1233-1238.

23) Kuduk, S.D.; Harris, C.R.; Zheng, F.F.; Sepp-Lorenzino, L.; Ouerfelli, Q.; Rosen, N.; Danishefsky, S.J. *Bioorg. Med. Chem. Lett.* **2000**, *10*, 1303-1306.

24) Chiosis, G.; Rosen, N.; Sepp-Lorenzino, L. *Bioorg. Med. Chem. Lett.* **2001**, *11*, 909-913.

25) Baselga, J. *Eur. J. Cancer* **2001**, *37* (Suppl.1), S18-S24.

26) Mandler, R.; Wu, C.; Sausville, E.A.; Roettinger, A.J.; Newman, D.J.; Ho, D.K.; King, C.R.; Yang, D.; Lippman, M.E.; Landolfi, N.F.; Dadachova, E.; Brechbiel, M.W.; Waldmann, T.A. *J. Natl. Cancer Inst.* **2000**, *92*, 1573-1581.

27) Mandler, R.; Kobayashi, H.; Hinson, E.R.; Brechbiel. M.W.; Waldmann, T.A. *Cancer Res.* **2004**, *64*, 1460-1467.

28) Qin, H. L.; Panek, J. S. *Org. Lett.* **2008**, *10*, 2477-2479.

29) Patel, K.; Piagentini, M.; Rascher, A.; Tian, Z-Q.; Buchanan, G.O.; Regentin, R.; Hu, Z.; Hutchinson, C.R.; McDaniel, R. *Chem. Biol.* **2004**, *11*, 1625-1633.

30) Neckers, L.; Lee, Y-S. *Nature* **2003**, *425*, 357-359.

31) Kamal, A.; Thao.; Sensintaffar, J.; Zhang, L.; Boehm, M.F.; Fritz, L.C.; Burrows, F.J. *Nature* **2003**, *425*, 407-410.

32) Kim, J.; Felts, S.; Llaugher, L.; He, H.; Huezo, H.; Rosen, N.; Chiosis, G. *Soc. for Biomol. Screen.* **2004**, *9*, 375-381.

33) Llauger-Bufi, L.; Felts, S.J.; Huezo, H.; Rosen, N.; Chiosis, G. *Bioorg. Med. Chem. Lett.* **2003**, *13*, 3975-3978.

34) Clevenger, R.C.; Rabiel, J.M.; Peck, A.M.; Blagg, B.S.J. *J. Org. Chem.* **2004**, *69*, 4375-4380.

35) Zhou, V.; Han, S.; Brinker, A.; Klock, H.; Caldwell, J.; Gu, X-J. *Anal. Biochem.* **2004**, *331*, 349-357.

36) Schulte, T.W.; Akinaga, S.; Soga, S.; Sullivan, W.; Stensgard, B.; Toft, D.; Neckers, L.M. *Cell Stress Chaperones* **1998**, *3*, 100–108.

37) Delmotte, P.; Delmotte-Plaque, J. *Nature* **1953**, *171*, 344-345.

38) Sharma, S.V.; Agatsuma, T.; Nakano, H. *Oncogene* **1998**, *16*, 2639-2645.

39) Chiosis, G.; Lucas, B.; Huezo, H.; Solit, D.; Basso, A.; Rosen, N. *Curr. Cancer Drug Targets* **2003**, *3*, 371-376.

40) Yamamoto, K.; Garbaccio, R.M.; Stachel, S.J.; Solit, D.B.; Chiosis, G.; Rosen, N.; Danishefsky, S.J. *Angew. Chem. Int. Ed.* **2003**, *42*, 1280-1284.

41) Cutler, H.G.; Arrendale, R.F.; Springer, J.P.; Cole, P.D.; Roberts, R.G.; Hanlin, R.T. *Agric. Biol. Chem.* **1987**, *51*, 3331-3338.

42) Geng, X.; Yang Z–Q.; Danishefsky, S.J. *Synlett* **2004**, *8*, 1325–1333.

43) Kwon, H.J.; Yoshida, M.; Fukui, Y.; Horinouchi, S.; Beppu, T. *Cancer Res.* **1992**, *52*, 6926-6930.

44) Soga, S.; Neckers, L.M.; Schulte, T.W.; Shiotsu, Y.; Akasaka, K.; Narumi, H.; Agatsuma, T.; Ikuina, Y.; Murakata, C.; Tamaoki, T.; Akinaga, S. *Cancer Res.* **1999**, *59*, 2931-2938.

45) Ikuina, Y.; Amishiro, N.; Miyata, M.; Narumi, H.; Ogawa, H.; Akiyama, T.; Shiotsu, Y.; Akinaga, S.; Murakata, C. *J. Med. Chem.* **2003**, *46*, 2534-2541.

46) Soga, S.; Sharma, S.; Shiotsu, Y.; Shimizu, M.; Tahara, H.; Yamaguchi, K.; Ikuina, Y.; Murakata, C.; Tamaoki, T.; Kurebayashi, J.; Schulte, T.W.; Neckers, L.M.; Skinaga, S. *Cancer Chemother. Pharmacol.* **2001**, *48*, 435-445.

47) Agatsuma, T.; Ogawa, H.; Akasaka, K.; Asai, A.; Yamashita, Y.; Mizukami, T.; Akinaga, S.; Saitoh, Y. *Bioorg. Med. Chem.* **2002**, *10*, 3445-3454.

48) Lampilas, M.; Lett, R. *Tetrahedron Lett.* **1992**, *33*, 773-780.

49) Garbaccio, R.M.; Stachel, S.J.; Baeschlin, D.K.; Danishefsky, S.J. *J. Am. Chem. Soc.* **2001**, *23*, 10903-10908.

50) Yang, Z.; Geng, X.; Solit, D.; Pratilas, C.A.; Rosen, N.; Danishefsky, S.J. *J. Am. Chem. Soc.* **2004**, *126*, 7881-7889.

51) Moulin, E.; Zoete, V.; Barluenga, S.; Karplus, M.; Winssinger, N. *J. Am. Chem. Soc.* **2005**, *127*, 6999-7004.

52) Moulin, E.; Barluenga, S.; Winssinger, N. *Org. Lett.* **2005**, *7*, 5637-5639.

53) Jez, J.M.; Chen, J.C–H.; Rastelli, G.; Stroud, R.M.; Santi, D.V. *Chem. Biol.* **2003**, *10*, 361–368.

54) Lee, Y–S.; Marcu, M.G.; Neckers, L.M. *Chem. Biol.* **2004**, *11*, 991–998.

55) Clevenger, R.C.; Blagg, B.S.J. *Org. Lett.* **2004**, *6*, 4459–4462.

56) Avila, C.; Kornilayev, B.A.; Blagg, B.S.J. *Bioorg. Med. Chem*. **2006**, *14*, 1134–1142.

57) Shen, G.; Blagg, B.S.J. *Org. Lett.* **2005**, *7*, 2157–2160.

58) Wang, M.; Shen, G.; Blagg, B.S.J. *Bioorg. Med. Chem. Lett*. **2006**, 2459-2462.

59) Marcu, M. G.; Schulte, T. W.; Neckers, L. *J. Nat. Cancer. Inst.* **2000**, *92*, 242-247.

60) Marcu, M. G.; Chadli, A.; Bouhouche, I.; Catelli, M.; Neckers, L. M. *J. Biol. Chem.* **2000**, *47*, 37181-37186.

61) Hadden, M. K.; Galam, L.; Matts, R. A.; Blagg, B. S. J. *J. Nat. Prod.* **2007**, *70*, 2014-2018.

62) Yu, X. M.; Shen, G.; Neckers, L.; Blake, H.; Holzbeierlein, J.; Cronk, B.; Blagg, B. S. J. *J. Am. Chem. Soc*. **2005**, *127*, 12778-12779.

63) Burlison, J. A.; Avila, C.; Vielhauer, G.; Lubbers, D. J.; Holzbeierlein, J.; Blagg, B. S. J. *J. Org. Chem.* **2008**, *73,* 2130-2137.

64) Burlison, J. A.; Neckers, L.; Smith, A. B.; Maxwell, A.; Blagg, B. S. J. *J. Am. Chem. Soc.* **2006**, *128*, 15529-15536.

65) Yu, X. M.; Shen, G.; Blagg, B. S. J. *J. Org. Chem.* **2004**, *69*, 7375-7378.

66) Morgan, J. P.; Grubbs, R. H. *Org. Lett.* **2000**, *2*, 3153-3155.

67) Humphries, P.; Do, Q.; Wilhite, D. *Beil. J. Org. Chem.* **2006**, *2*, 21-25.

68) Grochowski, E.; Hilton, B. D.; Kupper, R. J.; Michejda, C. J. *J. Am. Chem. Soc.* **1982**, *104*, 6876-6877.

69) Soo, E. T.; Yip, G. W.; Lwin, Z. M.; Kumar, S. D.; Bay, B. H. *In Vivo*. **2008**, *22*, 311-315.

70) Allan, R. K.; Mok, D.; Ward, B. K.; Ratajczak, T. *J. Biol. Chem*. **2006**, *281*, 7161-7171.

71) Shen, G.; Yu, X. M.; Blagg, B. S. J. *Bioorg. Med. Chem. Lett*. **2004**, *14*, 5903-5906.

72) Bron, P.; Giudice, E.; Rolland, J. P.; Buey, R. M.; Barbier, P.; Diaz, J.F.; Peyrot, V.; Thomas, D.; Garnier, C. *Biol. Cell*. **2008**, *100*, 413-425.

73) Krukenberg, K.A.; Förster, F.; Rice, L. M.; Sali, A.; Agard, D. A. *Structure.* **2008**, *16*, 755-765.

74) Halaimia, F.; Djerourou, A. H. *Comp. Rend. Chim.* **2006**, *9*, 141-147.

75) Avi, M.; Fechter, M. H.; Gruber, K.; Belaj, F.; Poechlauer, P.; Griengl, H. *Tetrahedron*. **2004**, *60*, 10411-10418.

76) Reagents ordered as from Sigma-Aldrich and used as received.

77) Pine, S.H.; Sanchez, B. L. *J. Org. Chem.* **1971**, *36*, 829-837.

78) Wawrzenczyk, C.; Lochynski, S. *Monat.Fuer Chim.* **1985**, *116*, 99-110.

Appendix

Molecular modeling. All protein models were built using version 1.0 Pymol comparative protein modeling open-source software from DeLano Scientific. Protein structure homology comparisons were done using SwissModel via the ExPASy web server. Initial models and sequences were adapted from two Protein Data Bank files: 2CGE, middle and C-terminal Hsp82 domains (residues 273-677); and 2CG9, full length Hsp82 structure (residues 1-677) with mutant region 221-LQHMASVD-255. Manual editing and conformational changes were done using PyMol in Windows and RedHat platforms.

Protein model structures were converted to Unix-based Sybyl molecular docking software version 7.1 and hybridization for individual atoms was corrected manually. Hydrogen atoms were added and charges calculated within the Sybyl program using the Gasteiger and Marsili methods for each protein model and ligand. All ligand structures were built using the "Draw" functionality in Sybyl, and structures were minimized via 10,000 iterations to overcome maxima/minima limitations. One hundred docks per ligand-protein interaction were included in each analysis using Sybyl version 7.1 and 8.0. Connolly surfaces and electronic interactions were analyzed using MOLCAD. The binding site coordinates from the most consistent model from each series are shown in PDB-compatible format (Model **M1P**, Table **A.1**; Model **3CT**, Table **A.2**; Model **EM1**, Table **A.3**).

Table A.1. Coordinates for Molecular Model **M1P** Binding Sites.

ATOM#	ATOM	AMINO ACID	RESIDUE#	COORDINATES		
3006	N	TYR	473	-53.021	15.684	9.482
3007	CA	TYR	473	-51.873	16.539	9.615
3008	C	TYR	473	-51.613	16.807	11.070
3009	O	TYR	473	-52.428	16.456	11.940
3010	CB	TYR	473	-52.061	17.856	8.865
3011	CG	TYR	473	-53.169	18.801	9.357
3012	CD1	TYR	473	-52.847	19.914	10.119
3013	CD2	TYR	473	-54.500	18.622	8.990
3014	CE1	TYR	473	-53.808	20.811	10.544
3015	CE2	TYR	473	-55.471	19.505	9.399
3016	CZ	TYR	473	-55.118	20.606	10.189
3017	OH	TYR	473	-56.084	21.495	10.619
3018	N	ILE	474	-50.449	17.403	11.319
3019	CA	ILE	474	-50.083	17.896	12.640
3020	C	ILE	474	-49.410	19.269	12.509
3021	O	ILE	474	-48.656	19.540	11.541
3022	CB	ILE	474	-49.208	16.922	13.411
3023	CG1	ILE	474	-48.727	17.574	14.680
3024	CG2	ILE	474	-48.045	16.419	12.573
3025	CD1	ILE	474	-48.444	16.564	15.800
3026	N	THR	475	-49.729	20.147	13.468
3027	CA	THR	475	-49.276	21.533	13.498
3028	C	THR	475	-48.344	21.714	14.669
3029	O	THR	475	-48.572	21.143	15.744

(continued)

Table A.1. (continued)

ATOM#	ATOM	AMINO ACID	RESIDUE#	COORDINATES		
3030	CB	THR	475	-50.453	22.401	13.710
3031	OG1	THR	475	-51.298	21.791	14.705
3032	CG2	THR	475	-51.195	22.521	12.398
3033	N	GLY	476	-47.285	22.487	14.479
3034	CA	GLY	476	-46.301	22.675	15.557
3035	C	GLY	476	-45.118	23.546	15.191
3036	O	GLY	476	-45.010	24.007	14.067
3037	N	GLU	477	-44.224	23.761	16.139
3038	CA	GLU	477	-43.139	24.710	15.961
3039	C	GLU	477	-42.303	24.511	14.696
3040	O	GLU	477	-42.178	25.409	13.877
3041	CB	GLU	477	-42.218	24.628	17.157
3042	CG	GLU	477	-41.696	25.946	17.564
3043	CD	GLU	477	-42.498	26.550	18.717
3044	OE1	GLU	477	-42.226	26.120	19.882
3045	OE2	GLU	477	-43.362	27.458	18.466
3046	N	SER	478	-41.710	23.332	14.570
3047	CA	SER	478	-40.792	23.000	13.501
3048	C	SER	478	-40.925	21.524	13.228
3049	O	SER	478	-41.605	20.816	13.959
3050	CB	SER	478	-39.363	23.263	13.950
3051	OG	SER	478	-38.932	22.260	14.854
3052	N	LEU	479	-40.255	21.049	12.189

(continued)

Table A.1. (continued)

ATOM#	ATOM	AMINO ACID	RESIDUE#	COORDINATES		
3053	CA	LEU	479	-40.220	19.627	11.903
3054	C	LEU	479	-39.653	18.872	13.100
3055	O	LEU	479	-40.295	17.962	13.604
3056	CB	LEU	479	-39.400	19.371	10.644
3057	CG	LEU	479	-39.480	18.036	9.908
3058	CD1	LEU	479	-39.762	18.269	8.443
3059	CD2	LEU	479	-38.197	17.308	10.067
3060	N	LYS	480	-38.482	19.274	13.575
3061	CA	LYS	480	-37.850	18.611	14.720
3062	C	LYS	480	-38.796	18.388	15.892
3063	O	LYS	480	-38.805	17.337	16.512
3064	CB	LYS	480	-36.658	19.424	15.214
3065	CG	LYS	480	-35.590	19.646	14.169
3066	CD	LYS	480	-34.355	20.293	14.781
3067	CE	LYS	480	-33.517	19.323	15.609
3068	NZ	LYS	480	-32.264	19.981	16.066
3069	N	ALA	481	-39.594	19.398	16.184
3070	CA	ALA	481	-40.461	19.381	17.338
3071	C	ALA	481	-41.648	18.440	17.112
3072	O	ALA	481	-42.021	17.645	18.001
3073	CB	ALA	481	-40.940	20.798	17.609
3074	N	VAL	482	-42.199	18.527	15.902
3075	CA	VAL	482	-43.439	17.897	15.530

(continued)

Table A.1. (continued)

ATOM#	ATOM	AMINO ACID	RESIDUE#	COORDINATES		
3076	C	VAL	482	-43.349	16.347	15.403
3077	O	VAL	482	-44.337	15.627	15.537
3078	CB	VAL	482	-43.989	18.608	14.266
3079	CG1	VAL	482	-43.930	17.735	13.019
3080	CG2	VAL	482	-45.384	19.103	14.508
3081	N	GLU	483	-42.171	15.808	15.186
3082	CA	GLU	483	-42.073	14.356	15.113
3083	C	GLU	483	-42.079	13.717	16.500
3084	O	GLU	483	-42.453	12.552	16.652
3085	CB	GLU	483	-40.824	13.941	14.349
3086	CG	GLU	483	-40.732	14.587	12.983
3087	CD	GLU	483	-39.330	14.542	12.387
3088	OE1	GLU	483	-38.310	14.486	13.141
3089	OE2	GLU	483	-39.257	14.576	11.140
4200	N	ILE	622	-52.012	4.523	34.839
4201	CA	ILE	622	-53.454	4.723	34.875
4202	C	ILE	622	-54.127	3.556	35.589
4203	O	ILE	622	-54.869	3.766	36.551
4204	CB	ILE	622	-54.031	4.973	33.462
4205	CG1	ILE	622	-53.854	6.431	33.083
4206	CG2	ILE	622	-55.495	4.691	33.411
4207	CD1	ILE	622	-52.453	6.779	32.881
4208	N	LYS	623	-53.831	2.336	35.137

(continued)

Table A.1. (continued)

ATOM#	ATOM	AMINO ACID	RESIDUE#	COORDINATES		
4209	CA	LYS	623	-54.343	1.110	35.770
4210	C	LYS	623	-54.309	1.203	37.292
4211	O	LYS	623	-55.243	0.784	37.981
4212	CB	LYS	623	-53.532	-0.105	35.331
4213	CG	LYS	623	-53.595	-0.422	33.844
4214	CD	LYS	623	-52.826	-1.702	33.529
4215	CE	LYS	623	-52.517	-1.865	32.033
4216	NZ	LYS	623	-53.696	-2.304	31.207
4217	N	GLU	624	-53.216	1.780	37.780
4218	CA	GLU	624	-52.960	1.989	39.190
4219	C	GLU	624	-53.890	3.021	39.838
4220	O	GLU	624	-54.405	2.798	40.941
4221	CB	GLU	624	-51.495	2.398	39.381
4222	CG	GLU	624	-51.125	2.745	40.819
4223	CD	GLU	624	-51.568	1.684	41.800
4224	OE1	GLU	624	-51.010	0.576	41.746
4225	OE2	GLU	624	-52.481	1.950	42.609
4226	N	LEU	625	-54.086	4.151	39.171
4227	CA	LEU	625	-54.981	5.168	39.693
4228	C	LEU	625	-56.418	4.643	39.803
4229	O	LEU	625	-57.142	4.970	40.759
4230	CB	LEU	625	-54.944	6.416	38.814
4231	CG	LEU	625	-53.837	7.440	39.004

(continued)

Table A.1. (continued)

ATOM#	ATOM	AMINO ACID	RESIDUE#	COORDINATES		
4232	CD1	LEU	625	-53.787	8.291	37.771
4233	CD2	LEU	625	-54.083	8.288	40.230
4234	N	LYS	626	-56.821	3.826	38.826
4235	CA	LYS	626	-58.129	3.175	38.859
4236	C	LYS	626	-58.221	2.380	40.136
4237	O	LYS	626	-59.209	2.468	40.851
4238	CB	LYS	626	-58.320	2.292	37.624
4239	CG	LYS	626	-59.685	1.630	37.539
4240	CD	LYS	626	-59.805	0.770	36.291
4241	CE	LYS	626	-61.171	0.108	36.207
4242	NZ	LYS	626	-61.388	-0.862	37.316
4243	N	LYS	627	-57.160	1.638	40.436
4244	CA	LYS	627	-57.138	0.762	41.607
4245	C	LYS	627	-57.431	1.518	42.889
4246	O	LYS	627	-58.268	1.086	43.695
4247	CB	LYS	627	-55.816	-0.013	41.721
4248	CG	LYS	627	-55.499	-0.923	40.530
4249	CD	LYS	627	-56.594	-1.962	40.274
4250	CE	LYS	627	-57.662	-1.458	39.286
4251	NZ	LYS	627	-58.949	-2.219	39.385
4252	N	ARG	628	-56.769	2.661	43.056
4253	CA	ARG	628	-56.916	3.433	44.277
4254	C	ARG	628	-58.316	4.019	44.383

(continued)

Table A.1. (continued)

ATOM#	ATOM	AMINO ACID	RESIDUE#	COORDINATES		
4255	O	ARG	628	-58.851	4.144	45.477
4256	CB	ARG	628	-55.843	4.504	44.373
4257	CG	ARG	628	-54.451	3.941	44.303
4258	CD	ARG	628	-53.531	4.668	45.239
4259	NE	ARG	628	-52.173	4.138	45.170
4260	CZ	ARG	628	-51.122	4.676	45.785
4261	NH1	ARG	628	-51.275	5.775	46.523
4262	NH2	ARG	628	-49.919	4.115	45.660
4263	N	VAL	629	-58.905	4.336	43.232
4264	CA	VAL	629	-60.275	4.863	43.140
4265	C	VAL	629	-61.315	3.790	43.461
4266	O	VAL	629	-62.265	4.029	44.212
4267	CB	VAL	629	-60.531	5.514	41.732
4268	CG1	VAL	629	-62.009	5.500	41.333
4269	CG2	VAL	629	-59.966	6.927	41.702
4270	N	ASP	630	-61.109	2.609	42.887
4271	CA	ASP	630	-61.945	1.433	43.139
4272	C	ASP	630	-61.719	0.927	44.556
4273	O	ASP	630	-62.097	-0.196	44.886
4274	CB	ASP	630	-61.624	0.320	42.123
4275	CG	ASP	630	-61.970	0.711	40.679
4276	OD1	ASP	630	-62.985	1.414	40.477
4277	OD2	ASP	630	-61.240	0.310	39.740

(continued)

Table A.1. (continued)

ATOM#	ATOM	AMINO ACID	RESIDUE#	COORDINATES		
4278	N	GLU	631	-61.086	1.768	45.375
4279	CA	GLU	631	-60.759	1.459	46.765
4280	C	GLU	631	-60.936	2.691	47.643
4281	O	GLU	631	-60.097	2.987	48.494
4282	CB	GLU	631	-59.330	0.917	46.868
4283	CG	GLU	631	-59.206	-0.552	46.459
4284	CD	GLU	631	-57.765	-1.012	46.253
4285	OE1	GLU	631	-56.921	-0.205	45.796
4286	OE2	GLU	631	-57.482	-2.198	46.536
4287	N	GLY	632	-62.034	3.410	47.409
4288	CA	GLY	632	-62.415	4.585	48.196
4289	C	GLY	632	-61.477	5.775	48.098
4290	O	GLY	632	-61.826	6.884	48.521
4291	N	GLY	633	-60.284	5.546	47.543
4292	CA	GLY	633	-59.253	6.586	47.398
4293	C	GLY	633	-59.582	7.669	46.380
4294	O	GLY	633	-58.694	8.141	45.662

Table A.2 Coordinates for Molecular Model **3CT** Binding Sites.

ATOM#	ATOM	AMINO ACID	RESIDUE#	COORDINATES		
3106	N	GLU	376	-78.639	-69.920	43.803
3107	CA	GLU	376	-78.719	-68.446	43.838
3108	C	GLU	376	-78.924	-67.876	42.427
3109	O	GLU	376	-79.823	-67.070	42.211
3110	CB	GLU	376	-77.417	-67.872	44.402
3111	CG	GLU	376	-77.195	-68.202	45.880
3112	CD	GLU	376	-77.928	-67.248	46.829
3113	OE1	GLU	376	-79.147	-67.025	46.646
3114	OE2	GLU	376	-77.240	-66.748	47.742
3115	N	THR	377	-78.207	-68.460	41.466
3116	CA	THR	377	-78.322	-68.082	40.043
3117	C	THR	377	-79.729	-68.369	39.509
3118	O	THR	377	-80.288	-67.540	38.784
3119	CB	THR	377	-77.275	-68.820	39.191
3120	OG1	THR	377	-75.978	-68.377	39.590
3121	CG2	THR	377	-77.448	-68.609	37.680
3122	N	ALA	378	-80.256	-69.541	39.832
3123	CA	ALA	378	-81.603	-69.954	39.400
3124	C	ALA	378	-82.650	-68.927	39.843
3125	O	ALA	378	-83.371	-68.419	39.001
3126	CB	ALA	378	-81.941	-71.325	39.976
3127	N	LEU	379	-82.525	-68.463	41.091
3128	CA	LEU	379	-83.348	-67.369	41.631

(continued)

Table A.2. (continued)

ATOM#	ATOM	AMINO ACID	RESIDUE#	COORDINATES		
3129	C	LEU	379	-83.310	-66.132	40.729
3130	O	LEU	379	-84.335	-65.710	40.245
3131	CB	LEU	379	-82.860	-66.960	43.021
3132	CG	LEU	379	-83.065	-68.054	44.066
3133	CD1	LEU	379	-82.329	-67.670	45.347
3134	CD2	LEU	379	-84.553	-68.224	44.381
3135	N	LEU	380	-82.103	-65.752	40.297
3136	CA	LEU	380	-81.967	-64.638	39.346
3137	C	LEU	380	-82.613	-64.914	37.994
3138	O	LEU	380	-83.586	-64.256	37.625
3139	CB	LEU	380	-80.511	-64.208	39.130
3140	CG	LEU	380	-79.935	-63.340	40.256
3141	CD1	LEU	380	-80.938	-62.309	40.794
3142	CD2	LEU	380	-79.311	-64.190	41.361
3143	N	SER	381	-82.151	-65.988	37.369
3144	CA	SER	381	-82.635	-66.415	36.043
3145	C	SER	381	-84.162	-66.589	36.016
3146	O	SER	381	-84.834	-66.087	35.113
3147	CB	SER	381	-81.971	-67.738	35.658
3148	OG	SER	381	-82.454	-68.150	34.378
3149	N	SER	382	-84.699	-67.172	37.075
3150	CA	SER	382	-86.141	-67.456	37.216
3151	C	SER	382	-86.929	-66.271	37.803
3152	O	SER	382	-88.083	-66.429	38.203

(continued)

Table A.2. (continued)

ATOM#	ATOM	AMINO ACID	RESIDUE#	COORDINATES		
3153	CB	SER	382	-86.340	-68.715	38.071
3154	OG	SER	382	-85.679	-69.829	37.454
3155	N	GLY	383	-86.314	-65.081	37.760
3156	CA	GLY	383	-86.935	-63.819	38.211
3157	C	GLY	383	-87.280	-63.813	39.705
3158	O	GLY	383	-88.451	-63.682	40.096
3159	N	PHE	384	-86.263	-63.929	40.516
3160	CA	PHE	384	-86.309	-63.821	41.987
3161	C	PHE	384	-85.138	-62.971	42.469
3162	O	PHE	384	-84.107	-62.857	41.794
3163	CB	PHE	384	-86.181	-65.190	42.668
3164	CG	PHE	384	-87.471	-66.002	42.698
3165	CD1	PHE	384	-88.341	-65.820	43.765
3166	CD2	PHE	384	-87.707	-67.006	41.764
3167	CE1	PHE	384	-89.449	-66.639	43.902
3168	CE2	PHE	384	-88.816	-67.829	41.904
3169	CZ	PHE	384	-89.688	-67.640	42.971
3170	N	SER	385	-85.350	-62.292	43.583
3171	CA	SER	385	-84.225	-61.746	44.361
3172	C	SER	385	-83.621	-62.913	45.155
3173	O	SER	385	-84.311	-63.888	45.487
3174	CB	SER	385	-84.668	-60.625	45.307
3175	OG	SER	385	-85.429	-61.168	46.382

(continued)

Table A.2. (continued)

ATOM#	ATOM	AMINO ACID	RESIDUE#	COORDINATES		
3176	N	LEU	386	-82.340	-62.832	45.425
3177	CA	LEU	386	-81.602	-63.927	46.080
3178	C	LEU	386	-81.621	-63.793	47.612
3179	O	LEU	386	-82.443	-63.090	48.197
3180	CB	LEU	386	-80.180	-64.013	45.503
3181	CG	LEU	386	-79.420	-62.686	45.606
3182	CD1	LEU	386	-77.925	-62.957	45.626
3183	CD2	LEU	386	-79.719	-61.791	44.402
3184	N	GLU	387	-80.647	-64.445	48.237
3185	CA	GLU	387	-80.514	-64.481	49.696
3186	C	GLU	387	-79.217	-63.858	50.166
3187	O	GLU	387	-78.197	-64.535	50.302
3188	CB	GLU	387	-80.615	-65.928	50.158
3189	CG	GLU	387	-82.068	-66.321	49.925
3190	CD	GLU	387	-83.044	-65.817	50.987
3191	OE1	GLU	387	-82.643	-64.963	51.811
3192	OE2	GLU	387	-84.183	-66.323	50.956
3193	N	ASP	388	-79.315	-62.556	50.416
3194	CA	ASP	388	-78.237	-61.796	51.071
3195	C	ASP	388	-77.016	-61.568	50.161
3196	O	ASP	388	-76.673	-62.428	49.340
3197	CB	ASP	388	-77.797	-62.474	52.385
3198	CG	ASP	388	-78.980	-62.628	53.340

(continued)

Table A.2. (continued)

ATOM#	ATOM	AMINO ACID	RESIDUE#	COORDINATES		
3199	OD1	ASP	388	-79.510	-61.567	53.731
3200	OD2	ASP	388	-79.334	-63.792	53.622
3201	N	PRO	389	-76.359	-60.420	50.352
3202	CA	PRO	389	-75.159	-60.018	49.600
3203	C	PRO	389	-74.017	-60.982	49.935
3204	O	PRO	389	-73.805	-61.918	49.193
3205	CB	PRO	389	-74.898	-58.576	50.041
3206	CG	PRO	389	-75.392	-58.551	51.489
3207	CD	PRO	389	-76.639	-59.426	51.417
3208	N	GLN	390	-73.332	-60.720	51.062
3209	CA	GLN	390	-72.272	-61.544	51.674
3210	C	GLN	390	-72.050	-62.910	51.014
3211	O	GLN	390	-71.340	-62.963	49.996
3212	CB	GLN	390	-72.541	-61.681	53.186
3213	CG	GLN	390	-73.932	-62.259	53.490
3214	CD	GLN	390	-74.107	-62.554	54.964
3215	OE1	GLN	390	-74.207	-61.627	55.748
3216	NE2	GLN	390	-74.171	-63.815	55.342

Table A.3. Coordinates for Molecular Model **EM1** Binding Sites.

ATOM#	ATOM	AMINO ACID	RESIDUE#	COORDINATES		
2286	N	LYS	273	23.858	10.667	34.892
2287	CA	LYS	273	23.451	9.298	34.532
2288	C	LYS	273	23.720	8.313	35.678
2289	O	LYS	273	22.833	7.544	36.062
2290	CB	LYS	273	24.218	8.847	33.284
2291	CG	LYS	273	23.796	7.454	32.805
2292	CD	LYS	273	22.338	7.447	32.346
2293	CE	LYS	273	21.873	6.068	31.879
2294	NZ	LYS	273	21.867	5.100	32.983
2295	N	THR	274	24.891	8.454	36.287
2296	CA	THR	274	25.277	7.638	37.460
2297	C	THR	274	24.360	7.880	38.662
2298	O	THR	274	23.891	6.907	39.270
2299	CB	THR	274	26.718	7.905	37.897
2300	OG1	THR	274	26.836	9.270	38.288
2301	CG2	THR	274	27.725	7.539	36.801
2302	N	LYS	275	23.968	9.121	38.888
2303	CA	LYS	275	23.034	9.499	39.967
2304	C	LYS	275	21.685	8.772	39.830
2305	O	LYS	275	21.047	8.440	40.824
2306	CB	LYS	275	22.769	11.004	39.981
2307	CG	LYS	275	24.005	11.835	40.329
2308	CD	LYS	275	23.672	13.331	40.388
2309	CE	LYS	275	22.683	13.680	41.507

(continued)

Table A.3. (continued)

ATOM#	ATOM	AMINO ACID	RESIDUE#	COORDINATES		
2310	NZ	LYS	275	23.245	13.403	42.838
2311	N	PHE	276	21.336	8.427	38.592
2312	CA	PHE	276	20.010	7.878	38.270
2313	C	PHE	276	20.056	6.363	38.208
2314	O	PHE	276	19.010	5.729	38.224
2315	CB	PHE	276	19.517	8.404	36.920
2316	CG	PHE	276	19.225	9.904	36.917
2317	CD1	PHE	276	19.959	10.814	37.675
2318	CD2	PHE	276	18.166	10.383	36.169
2319	CE1	PHE	276	19.680	12.156	37.708
2320	CE2	PHE	276	17.878	11.731	36.212
2321	CZ	PHE	276	18.626	12.633	36.960
2322	N	GLU	277	21.264	5.804	38.207
2323	CA	GLU	277	21.494	4.359	38.062
2324	C	GLU	277	20.568	3.526	38.955
2325	O	GLU	277	19.810	2.702	38.456
2326	CB	GLU	277	22.946	4.049	38.422
2327	CG	GLU	277	23.517	2.941	37.536
2328	CD	GLU	277	23.865	3.446	36.134
2329	OE1	GLU	277	22.972	4.031	35.480
2330	OE2	GLU	277	25.022	3.214	35.732
2331	N	ASN	278	20.528	3.873	40.244

(continued)

Table A.3. (continued)

ATOM#	ATOM	AMINO ACID	RESIDUE#	COORDINATES		
2332	CA	ASN	278	19.648	3.192	41.203
2333	C	ASN	278	18.161	3.334	40.892
2334	O	ASN	278	17.407	2.461	41.251
2335	CB	ASN	278	19.906	3.643	42.639
2336	CG	ASN	278	21.234	3.087	43.150
2337	OD1	ASN	278	22.121	3.821	43.551
2338	ND2	ASN	278	21.391	1.778	43.080
2470	N	VAL	295	16.630	3.472	30.495
2471	CA	VAL	295	17.796	4.364	30.372
2472	C	VAL	295	17.397	5.827	30.597
2473	O	VAL	295	16.229	6.202	30.452
2474	CB	VAL	295	18.510	4.171	29.014
2475	CG1	VAL	295	18.929	2.715	28.777
2476	CG2	VAL	295	17.687	4.684	27.826
2477	N	VAL	296	18.405	6.645	30.829
2478	CA	VAL	296	18.253	8.109	30.887
2479	C	VAL	296	18.594	8.654	29.496
2480	O	VAL	296	19.645	8.340	28.937
2481	CB	VAL	296	19.209	8.670	31.947
2482	CG1	VAL	296	19.323	10.194	31.911
2483	CG2	VAL	296	18.790	8.223	33.346
2484	N	SER	297	17.719	9.513	29.000
2485	CA	SER	297	17.949	10.153	27.699

(continued)

Table A.3. (continued)

ATOM#	ATOM	AMINO ACID	RESIDUE#	COORDINATES		
2486	C	SER	297	17.958	11.674	27.820
2487	O	SER	297	17.205	12.277	28.596
2488	CB	SER	297	16.881	9.690	26.704
2489	OG	SER	297	17.208	10.156	25.392
2537	N	PRO	304	8.162	13.094	30.377
2538	CA	PRO	304	8.698	12.182	31.406
2539	C	PRO	304	9.588	11.081	30.855
2540	O	PRO	304	10.794	10.987	31.129
2541	CB	PRO	304	7.466	11.561	32.081
2542	CG	PRO	304	6.228	12.209	31.457
2543	CD	PRO	304	6.706	13.209	30.403
2544	N	CYS	305	8.936	10.303	30.027
2545	CA	CYS	305	9.468	9.068	29.472
2546	C	CYS	305	9.019	8.919	28.024
2547	O	CYS	305	8.109	9.622	27.553
2548	CB	CYS	305	8.957	7.902	30.323
2549	SG	CYS	305	7.133	7.789	30.344
2550	N	CYS	306	9.670	8.002	27.352
2551	CA	CYS	306	9.318	7.592	25.982
2552	C	CYS	306	9.938	6.229	25.702
2553	O	CYS	306	10.729	5.714	26.507
2554	CB	CYS	306	9.811	8.625	24.960
2555	SG	CYS	306	11.621	8.598	24.748

(continued)

Table A.3. (continued)

ATOM#	ATOM	AMINO ACID	RESIDUE#	COORDINATES		
5832	N	ARG	703	-1.844	24.996	32.143
5833	CA	ARG	703	-2.750	24.300	31.219
5834	C	ARG	703	-2.050	23.983	29.886
5835	O	ARG	703	-2.664	23.654	28.877
5836	CB	ARG	703	-3.939	25.223	30.966
5837	CG	ARG	703	-4.816	25.383	32.208
5838	CD	ARG	703	-6.076	26.174	31.866
5839	NE	ARG	703	-5.741	27.548	31.443
5840	CZ	ARG	703	-6.612	28.450	30.991
5841	NH1	ARG	703	-7.900	28.152	30.870
5842	NH2	ARG	703	-6.204	29.674	30.684
5843	N	LEU	704	-0.725	24.100	29.906
5844	CA	LEU	704	0.080	23.874	28.713
5845	C	LEU	704	1.305	22.996	29.046
5846	O	LEU	704	2.035	23.191	30.018
5847	CB	LEU	704	0.220	25.274	28.083
5848	CG	LEU	704	1.113	25.342	26.848
5849	CD1	LEU	704	0.665	24.447	25.702
5850	CD2	LEU	704	1.509	26.786	26.499
5851	N	VAL	705	1.297	21.827	28.427
5852	CA	VAL	705	2.307	20.791	28.717
5853	C	VAL	705	3.261	20.612	27.536
5854	O	VAL	705	2.842	20.595	26.376

(continued)

Table A.3. (continued)

ATOM#	ATOM	AMINO ACID	RESIDUE#	COORDINATES		
5855	CB	VAL	705	1.606	19.472	29.093
5856	CG1	VAL	705	0.775	18.926	27.937
5857	CG2	VAL	705	2.584	18.395	29.568
5858	N	THR	706	4.523	20.397	27.886
5859	CA	THR	706	5.594	20.003	26.941
5860	C	THR	706	5.557	20.773	25.608
5861	O	THR	706	5.603	20.206	24.525
5862	CB	THR	706	5.576	18.488	26.672
5863	OG1	THR	706	4.305	18.102	26.134
5864	CG2	THR	706	5.897	17.690	27.940
5865	N	SER	707	5.324	22.075	25.726
5866	CA	SER	707	5.304	22.948	24.542
5867	C	SER	707	5.676	24.347	25.019
5868	O	SER	707	5.139	24.780	25.998
5869	CB	SER	707	3.919	22.980	23.889
5870	OG	SER	707	3.988	23.768	22.698
5871	N	PRO	708	6.615	25.036	24.382
5872	CA	PRO	708	7.100	26.349	24.849
5873	C	PRO	708	5.992	27.328	25.202
5874	O	PRO	708	5.812	27.759	26.351
5875	CB	PRO	708	7.935	26.911	23.688
5876	CG	PRO	708	7.972	25.844	22.593
5877	CD	PRO	708	7.155	24.646	23.082